

UNCLASSIFIED

AD NUMBER

ADB017183

LIMITATION CHANGES

TO:

Approved for public release; distribution is unlimited.

FROM:

Distribution authorized to U.S. Gov't. agencies only; Proprietary Information; DEC 1976. Other requests shall be referred to Air Force Wright Aeronautics Lab., Wright-Patterson AFB, OH 45433.

AUTHORITY

AFWAL ltr 19 Oct 1981

THIS PAGE IS UNCLASSIFIED

THIS REPORT HAS BEEN DELIMITED
AND CLEARED FOR PUBLIC RELEASE
UNDER DOD DIRECTIVE 5200.20 AND
NO RESTRICTIONS ARE IMPOSED UPON
ITS USE AND DISCLOSURE.

DISTRIBUTION STATEMENT A

APPROVED FOR PUBLIC RELEASE,
DISTRIBUTION UNLIMITED.

AFAL-TR-75-231



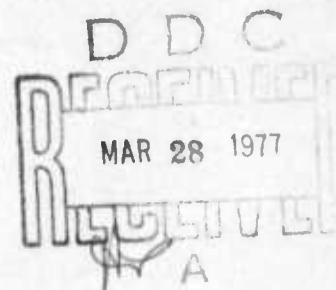
AD NO. 17183

ADVANCED SLIT DETECTORS

HONEYWELL RADIATION CENTER
HONEYWELL CORPORATE RESEARCH CENTER

DECEMBER 1976

TECHNICAL REPORT AFAL-TR-75-231
FINAL REPORT FOR PERIOD 15 APRIL 1974 through 12 SEPTEMBER 1975



28 MAR 1977

Distribution limited to U.S. Government agencies only due to proprietary information. The requests for this document must be referred to AFAL/DHO, WPAFB, OH 45433

AIR FORCE AVIONICS LABORATORY
AIR FORCE WRIGHT AERONAUTICAL LABORATORIES
AIR FORCE SYSTEMS COMMAND
WRIGHT-PATTERSON AIR FORCE BASE, OHIO 45433

NOTICE

When Government drawings, specifications, or other data are used for any purpose other than in connection with a definitely related Government procurement operation, the United States Government thereby incurs no responsibility nor any obligation whatsoever; and the fact that the government may have formulated, furnished, or in any way supplied the said drawings, specifications, or other data, is not to be regarded by implication or otherwise as in any manner licensing the holder or any other person or corporation, or conveying any rights or permission to manufacture, use, or sell any patented invention that may in any way be related thereto.

23 MAR 1977
Distribution limited to U.S. Government agencies only, due to proprietary information. The requests for this document must be referred to AFAL/DHO-3, Wright-Patterson AFB, Ohio 45433.

This technical report has been reviewed and is approved for publication.

Larry F. Reitz
LARRY F. REITZ, Project Engineer
Electro-Optic Detectors Group
Electro-Optics Technology Branch

Donald J. Peacock
DONALD J. PEACOCK, Actg. Chief
Electro-Optic Detectors Group
Electro-Optics Technology Branch

FOR THE COMMANDER

Edwin B. Champagne
EDWIN B. CHAMPAGNE, Actg. Chief
Electro-Optics Technology Branch
Electronic Technology Division

Copies of this report should not be returned unless return is required by security considerations, contractual obligations, or notice on a specific document.

UNCLASSIFIED

SECURITY CLASSIFICATION OF THIS PAGE (When Data Entered)

REPORT DOCUMENTATION PAGE		READ INSTRUCTIONS BEFORE COMPLETING FORM	
1. REPORT NUMBER AFAL-TR-75-231	2. GOVT ACCESSION NO.	3. RECIPIENT'S CATALOG NUMBER 15 Apr 74 - 12 Sep 75	
4. TITLE (and Subtitle) ADVANCED SLIT DETECTORS	5. TYPE OF REPORT & PERIOD COVERED FINAL 4/15/74 through 9/12/75		
7. AUTHOR(s) Alice Chiang Ralph Rotolante		8. CONTRACT OR GRANT NUMBER(s) F33615-74-C-1121 NEW	
9. PERFORMING ORGANIZATION NAME AND ADDRESS Honeywell Radiation Center 2 Forbes Rd. Lexington, MA 02173		10. PROGRAM ELEMENT, PROJECT, TASK AREA & WORK UNIT NUMBERS 62204F-2001-03-34	
11. CONTROLLING OFFICE NAME AND ADDRESS Air Force Avionics Laboratory (DHO-3) Air Force Systems Command Wright-Patterson Air Force Base, Ohio 45433		12. REPORT DATE December 1976	
14. MONITORING AGENCY NAME & ADDRESS (if different from Controlling Office)		13. NUMBER OF PAGES 66	
		15. SECURITY CLASS. (of this report) UNCLASSIFIED	
		15a. DECLASSIFICATION/DOWNGRADING SCHEDULE	
16. DISTRIBUTION STATEMENT (of this Report) Distribution limited to U.S. Government agencies only due to proprietary information. The requests for this document must be referred to AFAL/DHO-3, WPAFB, Ohio 45433			
17. DISTRIBUTION STATEMENT (of the abstract entered in Block 20, if different from Report)			
18. SUPPLEMENTARY NOTES			
19. KEY WORDS (Continue on reverse side if necessary and identify by block number) Photo Detectors GaP Detector Testing GaP Photoconductors			
20. ABSTRACT (Continue on reverse side if necessary and identify by block number) The specific objectives of this program were to fabricate, characterize and deliver forty gallium phosphide photoconduc- tive slit detectors (0.05 x 0.0005 inch) and subject 35 of these detectors to a series of environmental tests; temperature cycle, humidity, vibration, solar exposure, thermal vacuum, electron irradiation, proton irradiation, and gamma ray			

DD FORM 1473 1 JAN 73 EDITION OF 1 NOV 65 IS OBSOLETE

UNCLASSIFIED

SECURITY CLASSIFICATION OF THIS PAGE (When Data Entered)

59 in

over
bpg

UNCLASSIFIED

SECURITY CLASSIFICATION OF THIS PAGE(When Data Entered)

exposure before delivery. Each detector was characterized for sensitivity, noise, dark resistance, speed of response and spectral response prior to and after each environmental exposure. Overall, these detectors have clearly demonstrated the capability of high sensitivity, sufficient speed and high tolerance to severe environmental conditions for future use in a strapdown stellar sensor.

UNCLASSIFIED

SECURITY CLASSIFICATION OF THIS PAGE(When Data Entered)

FOREWORD

This is the Final Technical Report of the GaP Environmental Testing Program. This program was sponsored by the Air Force Systems Command, Air Force Avionics Laboratory, Wright-Patterson Air Force Base, Ohio, under Contract No. F33615-74-C-1121. This work was performed during the period April 15, 1974 through September 12, 1975. The Project Engineer was Dr. R. A. Rotolante. Principal investigator was Dr. A. Chiang. Research Scientists were Drs. F. Pribble, P. Petersen and R. Schulze. The Program Manager was J. R. Farrell. Acknowledgements are due to Air Force Cambridge Research Laboratory, where the gamma ray exposure, the electron, proton irradiation and vibration tests were performed. Thanks are also due to Mrs. M. Young who fabricated most of the slit detectors and Mr. R. Healey who obtained most of the test data. The Program Contract Monitors, Mr. Larry Reitz and Mr. Charles Ennis, provided considerable technical direction and supporting data during the course of the program.

RECEIVED BY
 NAME
 ADDRESS
 CITY
 STATE
 ZIP
 BY
 POSTAGE PAID
 PERMIT NO. 1000
 NEW YORK, N.Y. 10001
 POST OFFICE BOX 1000
 NEW YORK, N.Y. 10001

TABLE OF CONTENTS

SECTION		PAGE
I	INTRODUCTION.....	1
II	TECHNICAL DISCUSSION.....	3
	2.1 MATERIAL REQUIREMENT AND PREPARATION.....	3
	2.1.1 Material Requirement.....	3
	2.1.2 Material Preparation.....	4
	2.2 DETECTOR FABRICATION AND TESTING	
	PROCEDURES.....	9
	2.2.1 Detector Fabrication.....	9
	2.2.2 Detector Preselection and Testing	
	Procedures.....	11
	2.3 DETECTOR CHARACTERIZATION.....	13
	2.3.1 Dark Current-Voltage Measurement...	13
	2.3.2 Spot Scan Sensitivity.....	13
	2.3.3 Noise Measurements.....	16
	2.3.4 Rise and Fall Time.....	21
	2.3.5 Spectral Response.....	27
	2.3.6 Photoconductive Gain Measurement...	27
	2.3.7 Detector Uniformity.....	32
	2.3.8 Linearity of the Detector Response.	32
	2.3.9 Optimum Bias Point.....	32
	2.4 DETECTOR PERFORMANCE SUMMARY SHEET.....	32
III	ENVIRONMENTAL TEST RESULTS.....	41
	3.1 TEMPERATURE CYCLE.....	41
	3.2 VIBRATION.....	41
	3.3 HUMIDITY.....	43
	3.4 SOLAR EXPOSURE.....	43
	3.5 ELECTRON IRRADIATION.....	43
	3.6 PROTON IRRADIATION.....	48
	3.7 GAMMA RAY EXPOSURE.....	48
	3.8 THERMAL VACUUM.....	52
IV	SUMMARY.....	64
	APPENDIX	65
	REFERENCES.....	66

LIST OF ILLUSTRATIONS

FIGURE		PAGE
1	TRADEOFF BETWEEN DETECTOR PHOTOCONDUCTIVE GAIN AND DETECTOR RESISTANCE.....	5
2	GaP PHOTOCONDUCTIVE DETECTOR FABRICATION PROCEDURE.....	10
3	GaP SLIT DETECTOR TESTING PROCEDURE.....	12
4	CURRENT VS APPLIED VOLTAGE OF A GaP PC SLIT DETECTOR.....	14
5	CURRENT VS APPLIED VOLTAGE OF A GaP PC SLIT DETECTOR.....	15
6	COMPARISON OF SPECTRAL IRRADIANCE OF AO CLASS STAR VEGA AND A LABORATORY SIMULATED SOURCE.....	17
7	SPOT SCAN SENSITIVITY.....	18
8	GaP PREAMPLIFIER.....	19
9	SYSTEM GAIN PROFILE.....	20
10	DETECTOR WIDEBAND NOISE.....	22
11	NOISE SPECTRA OF THE SLIT DETECTOR.....	23
12	NOISE SPECTRUM OF THE SLIT DETECTOR.....	24
13	DETECTOR RISE AND FALL TIME.....	25
14	(a) TIME-DEPENDENT RESPONSE OF A GaP:Cu SAMPLE TO A SERIES OF 100-ms PULSES AT 10-s INTERVALS OF 2.8-eV RADIATION. (b) RESPONSE OF THE SAME SAMPLE TO A REGULARLY MODULATED SOURCE.....	26
15	DETECTOR PULSE RESPONSE.....	28
16	GaP PC SET DETECTOR RELATIVE SPECTRAL RESPONSE...	29
17	GaP PC SLIT DETECTOR RELATIVE SPECTRAL RESPONSE..	30
18	GaP PC SLIT DETECTORS RELATIVE SPECTRAL RESPONSE.	31
19	SPOT SCAN UNIFORMITY ALONG THE SLIT LENGTH.....	34
20	SPOT SCAN UNIFORMITY ALONG THE SLIT LENGTH.....	35
21	DETECTOR RESPONSE VS INPUT POWER.....	36
22	DETECTOR RESPONSE VS INPUT POWER.....	37

LIST OF ILLUSTRATIONS continued

FIGURE		PAGE
23	GaP LINEARITY DATA.....	38
24	OPTIMUM BIAS POINT OF THE SLIT DETECTOR.....	39
25	DETECTOR DECAY TIME AFTER SOLAR EXPOSURE.....	45
26	DETECTOR/PREAMP TESTING AT AFCRL CO-60 SOURCE.....	51
27	DETECTOR RESPONSE TO A GAMMA EVENT.....	53
28	DETECTOR NOISE VS GAMMA FLUX.....	54
29	DETECTOR EVENT RATE VS GAMMA FLUX.....	55
30	DETECTOR DARK RESISTANCE VS GAMMA FLUX.....	56
31	THERMAL VACUUM TEST TEMPERATURE PROFILE.....	58
32	DETECTOR SIGNAL DURING THERMAL VACUUM TEST.....	62

LIST OF TABLES

TABLE		PAGE
1	DETECTOR AD18M1A No. 2 - $R_F = 2.3 \times 10^{10} \Omega$, $V_{bias} = 20V$, $P_{in} = 8.4 \times 10^{-13}$ watts, SCANNING RATE = 0.75 mils/s.....	33
2	35 GaP SLIT DETECTORS PERFORMANCE SUMMARY CHART...	40
3	TEMPERATURE CYCLE TEST RESULTS.....	42
4	HUMIDITY TEST.....	44
5	DETECTOR PERFORMANCE BEFORE AND AFTER SOLAR EXPOSURE.....	47
6	DETECTOR PERFORMANCE BEFORE AND AFTER ELECTRON FLUENCE OF 10^{15} e/cm ²	49
7	DETECTOR PERFORMANCE BEFORE AND AFTER PROTON FLUENCE OF 10^{11} p/cm ²	50
8	GAMMA RADIATION EXPOSURE	57
9	DARK RESISTANCE MEASUREMENT AT THERMAL VACUUM TEST	59

SECTION I

INTRODUCTION

This is the final technical report under AFAL Contract No. F33615-74-C-1121. The specific objectives of this program were to fabricate, characterize and deliver forty gallium phosphide photoconductive slit detectors ($0.05 \times 0.0005 \text{ inch}^2$) and subject 35 of these detectors to a series of environmental tests; temperature cycle, humidity, vibration, solar exposure, thermal vacuum, electron irradiation, proton irradiation, and gamma ray exposure before delivery. Each detector was characterized for sensitivity, noise, dark resistance, speed of response and spectral response prior to and after each environmental exposure.

The work effort under this contract resulted in the production, test and delivery of forty high performance photoconductive gallium phosphide detectors. The high sensitivity detectors were fabricated from Cu-doped, n-type GaP single crystals grown from solution. Copper is a deep lying acceptor in GaP which can be used to produce compensated material of high resistivity and acts as a sensitizing center. These centers are minority carrier traps which result in a longer electron lifetime and high photoconductive gain. The details of operation and initial development of Cu-doped GaP photoconductors are described in Reference 1. The Cu-doped GaP slit detectors were shown to be capable of measuring a laboratory simulated A0 star of +7.5 magnitude ($2 \frac{1}{2}$ -inch clear aperture) with signal to rms noise ratio of 17 which corresponds to an NEP of $5 \times 10^{-16} \text{ watts}/\sqrt{\text{Hz}}$. Detector rise and fall times less than 100 ms have also been observed. Most of the 35 detectors subjected to the environmental tests were able to operate without any degradation after severe environmental tests. The only test failures attributed to a detector occurred at the last stage (290°F) of the temperature cycle and two other failures occurred at the humidity test. Both of them resulted from the low melting point of indium which was used as an interconnection material between the contact metal (Te/Ag/Ni) and the gold wire bonds. Overall, these detectors have clearly demonstrated the capability of high sensitivity, sufficient speed and high tolerance to environmental conditions for future use in a strap-down stellar sensor.

The material requirements and preparation and device fabrication and characterization are discussed in detail in Section II of this report. The results of the environmental tests are presented in Section III.

Some of the device development and material growth effort reported in this document was under AFAL Contract No. F33615-C-75-1041.

SECTION II

TECHNICAL DISCUSSION

The technical discussion is divided into three major sections; material requirement of Cu-doped GaP for star sensor applications, detector fabrication and testing procedures, and finally detector characterization.

GaP is a large bandgap semiconductor material ($E_{g\text{indirect}} = 2.25 \text{ eV}$). Cu-sensitized GaP operating in the photoconductive mode yields a high sensitivity device because of the photoconductive gain due to the trapping of minority carriers. The first part of this section discusses the major material parameter considerations in the design of detectors which are capable of meeting the program goal. Under AFAL Contract Nos. F33615-74-C-1121 and F33615-75-C-1041, a photolithographic technique was developed for the fabrication of gallium phosphide photoconductive slit detectors ($0.05 \times 0.0005 \text{ inch}^2$) from Cu-doped material. A detailed description of detector fabrication and the detector preselection procedures will be found in Section 2.2. Finally, methods used to characterize the performance of detectors are described in Section 2.3.

2.1 MATERIAL REQUIREMENT AND PREPARATION

2.1.1 Material Requirement

During the program, Cu-doped solution grown GaP material was used to fabricate highly sensitive photoconductive slit detectors. Copper is a deep lying acceptor which can be used to produce compensated material of high resistivity and acts as a sensitizing center.^(1,2,3,4) The sensitizing centers are minority carrier traps which result in a long electron lifetime and high photoconductive gain.

The performance design goal of the slit detectors for the star sensor application under AFAL Contract No. F33615-75-C-1041 was a peak signal to rms noise ratio of 10 to 1 for a signal energy of 6×10^{-14} watts (integrated detector energy). A tradeoff between the material resistivity and the detector photoconductive gain requirements such that the detector is

capable of meeting the design goals, has been carried out as follows. The signal current can be written as:

$$i_s = \eta F q G$$

where

η = quantum efficiency of the device

F = number of incident photons per second (1.5×10^5 ph/s at $0.5 \mu\text{m}$ based on the spec)

G = photoconductive gain

Let us consider the case that the detector thermal noise is the dominant noise source, the noise current per unit bandwidth can be written as:

$$i_N = \left(\frac{4kT}{R_D} \right)^{1/2}$$

where R_D is the detector resistance. It is straightforward to calculate that for $R_D = 10^{10}$ ohm and $\eta = 0.5$, a gain of one will meet the performance specification. However, if $R_D = 10^7$ ohm, a gain of 33 is required. The photoconductive gain required to meet the specification vs detector resistance is plotted in Figure 1, assuming a detector thermal noise limited case. It is easy to see the importance of using high resistivity* material which will yield a detector with lower detector noise and therefore less gain required to meet the design goal.

2.1.2 Material Preparation

Under AFAL Contract Nos. F33615-74-C-1121 and F33615-74-C-1041, ten copper-doped gallium phosphide (GaP) growth runs, AD-18 through AD-27 were completed and evaluated via Hall and photoelectric measurements.

*The relation between the detector dark resistance and resistivity of the bulk material is based on the relation $R_D = 2.8 \rho_D$; see the derivation in Appendix A.

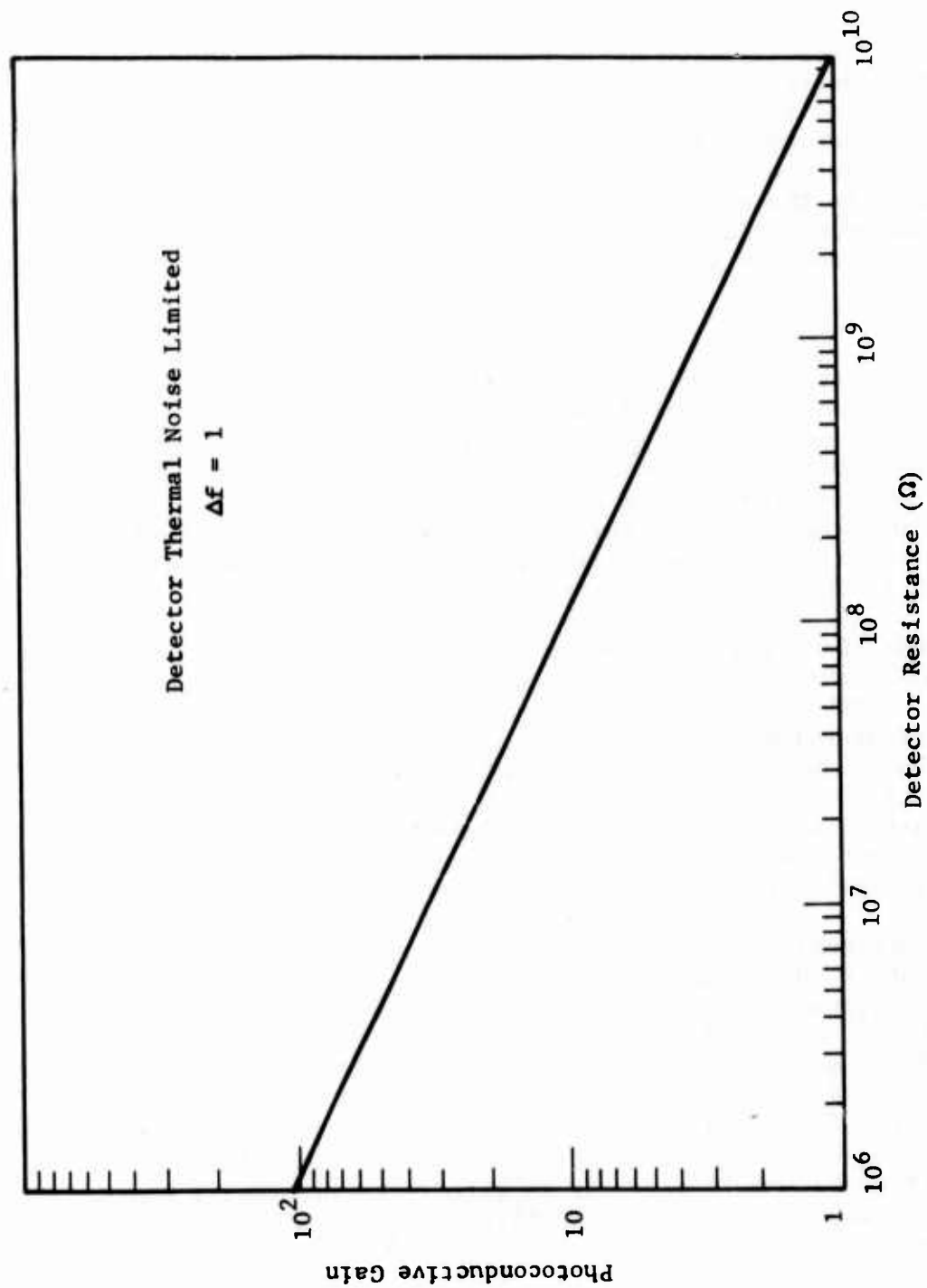


Figure 1 TRADEOFF BETWEEN DETECTOR PHOTOCONDUCTIVE GAIN AND DETECTOR RESISTANCE

Recrystallization AD-18 produced the first high resistivity n-type material resulting from recrystallizations performed under the current program. The run utilized starting GaP from Imanco Czochralski ingot one with a copper addition of 5.0 mole percent. Electrical measurements indicated the material was n-type with resistivities in the order of 1×10^6 to $1 \times 10^8 \Omega\text{-cm}$. Subsequent photoelectric measurements upon detectors fabricated from the material possessed gains of 80-90 with a response time less than 1 second.

Recrystallization AD-19 utilized starting material (Monsanto, lot one, 0.7 mole % Cu) which had been used previously and yielded p-type $100 \Omega\text{-cm}$ material. Hall data obtained from AD-19 allowed the calculation of the activation energy of the material. The value obtained indicated a departure from the values of the activation energies obtained for earlier recrystallized materials.⁽¹⁾ The low value of the activation energy indicates that an acceptor in addition to the copper was introduced into the crystal structure.

Run AD-20 was intended to be a duplication of recrystallization AD-18 which yielded n-type material possessing a resistivity of 1×10^6 - $1 \times 10^8 \Omega\text{-cm}$. Sections of Imanco ingot one were used as starting material with a copper addition of 5.0 mole percent. The resulting GaP was p-type with a resistivity of approximately $1000 \Omega\text{-cm}$. Initially, it was concluded the transition from n-type to p-type was rather abrupt. However, additional Hall measurements and calculation of the activation energy of the material again indicated an abnormal value.

Recrystallization AD-21 was the first copper-doped run employing lot two Monsanto starting material. A previous undoped recrystallization (AU-16) indicated a residual carrier (donor) concentration of $\sim 5 \times 10^{15} \text{cm}^{-3}$. Run AD-21 utilized a copper addition of 0.4 mole percent. The resulting material was p-type, possessing a resistivity of $\sim 100 \Omega\text{-cm}$. Again the activation energy deviated from those possessed by materials from recrystallizations prior to run AD-19. The additional acceptor has not been identified but could possibly be zinc. The procedures were analyzed, but the origin of the possible zinc contamination was not apparent.

In recrystallization AD-22, an attempt was made to approach compensation of the Imanco ingot material from the n-type side. The copper addition was lowered from 5.0 mole percent to

4.0 mole percent. The resulting material was n-type possessing resistivities over the range of 1×10^3 to $1 \times 10^{10} \Omega\text{-cm}$. The crystals produced were small in size.

The yield of larger size crystals appears to be influenced by the rate of growth and temperature range over which precipitation occurs. Slower precipitation rates and longer growth periods (wider temperature range of precipitation) are more efficient in producing large crystals. The recrystallization AD-23 utilized the second lot of Monsanto polycrystalline GaP as starting material. The residual carrier concentration was inferred from Hall measurements performed on a crystal from an undoped run (AU-16). The data indicated a carrier (donor) concentration of approximately $5 \times 10^{15} \text{ cm}^{-3}$. The copper concentration employed in run AD-23 was 0.2 mole percent and an extended temperature range of precipitation was utilized (1150-1000°C). The resulting material was p-type possessing a resistivity of approximately $1 \times 10^3 \Omega\text{-cm}$. The consistent growth of p-type material when employing Monsanto lot two starting GaP and activation energy calculations tend to indicate an additional unknown acceptor is being introduced during the growth process. Possibly, it is most evident in the Monsanto material because of its low residual carrier concentration. If the unknown acceptor was being inadvertently introduced in quantities equal to the concentration of the residual carrier, p-type material would be expected. The addition of copper will assure p-type material. Previous data (although minimal) tended to indicate the introduction of the unknown acceptor was associated with the addition of copper to the melt. Undoped recrystallizations employing Monsanto GaP yield n-type material with expected activation energies.

Recrystallizations AD-24 and AD-25 had similar growth parameters. Copper was added in the amount of 4.2 mole percent. The growths were terminated (air quenched) at 1080°C. The recrystallizations employed starting material from Imanco Czochralski ingot one. Preliminary data indicated material of high resistivities ($10^6 - 10^8 \Omega\text{-cm}$). Photoelectric measurements on a few samples indicated satisfactory photodetector characteristics.

Recrystallization AD-26 is the initial recrystallization employing a new starting material (Imanco Czochralski ingot two). The Hall characteristics of the two ingots are not identical. Ingot two possessed a somewhat higher residual carrier concentration and a lower resistivity than ingot one. Further, optical

absorption data indicated nearly equivalent sulfur and silicon concentrations. Ingot one possessed sulfur as the primary impurity (material was nominally undoped) with silicon being present in concentrations about an order of magnitude lower ($2-4 \times 10^{15} \text{ cm}^{-3}$).

The quantity of copper added to the solution in recrystallization AD-26 was 4.2 mole percent. The starting material was taken from the seed end of the ingot to obtain a residual carrier concentration ($\sim 5.0 \times 10^{16} \text{ cm}^{-3}$) near that ($3.9 \times 10^{16} \text{ cm}^{-3}$) of the seed end of ingot one. Seed end material from ingot one yielded two consecutive runs of photo-detector quality material (AD-24, AD-25).

Recrystallization AD-26 yielded n-type material of which two Hall samples indicated resistivities of 10 Ω -cm and 50 Ω -cm (starting material resistivity = 0.7402 Ω -cm). Since the resistivity of the material was low, it was concluded the material did not have adequate photoresponse for the fabrication of detectors.

The AD-27 run was accomplished to bracket the concentrations of copper required to produce n- and p-type material. Recrystallization AD-26 yielded low (10-50 Ω -cm) resistivity n-type material while AD-27 yielded high ($1 \times 10^4 \Omega$ -cm) p-type copper-doped gallium phosphide. These data suggest that 7.5 mole percent copper is near the concentration required for close compensation of ingot two material.

Recrystallization AD-27 differed from recrystallization AD-26 in that temperature instabilities were introduced during the first 48 hours of growth and a temperature rise (about 2°C) was inadvertently introduced during the early part of the growth cycle (shortly after the 48-hour period). The predominant type of growth in AD-26 was surface growth while in AD-27, the growth was confined to one end of the growth container and the crystals formed in the interior of the solution. Run AD-27 yielded two larger crystals (irregular shaped, approximately 0.250" x 0.375")

and a number of somewhat smaller crystals, even though the growth was quenched at a relatively high temperature (1078°C).

Hall samples (two) were prepared from the large crystals and measurements indicated similar resistivities ($\sim 1 \times 10^4 \Omega\text{-cm}$).

2.2 DETECTOR FABRICATION AND TESTING PROCEDURES

2.2.1 Detector Fabrication

During these two programs, a photolithographic procedure was developed to fabricate a radial GaP array (detector element size: $0.05 \times 0.0005 \text{ inch}^2$). The fabrication procedures used in the present program were evolved from those used in Phase I and Phase II programs. Several improvements were developed. A sequence of the fabrication procedure is shown schematically in Figure 2.

The as-received Cu-doped gallium phosphide crystal material is in the form of platelets and prism-shaped pieces. In step 2, Figure 2, the thickness uniformity over the surface area (back and front) of the pieces is achieved by mechanical lapping procedures. The crystal pieces are supported with bees-wax on stainless steel lapping blocks during the lapping operation. Sequential lapping of the surface was performed with slurries of W-8 garnet. The final lapping of the surface was carried out on a suspension of 3- μm aluminum oxide particles in water and glycerine. Relative smooth and pitless pieces with parallel surfaces were obtained in this manner. A sequence of organic solvents and detergent solutions were used to remove the residual wax film and adherent abrasive particles on the surface. The surface damage left after the mechanical lapping operation is removed by chemical etching, shown in step 3. The etch solution used is a diluted aqua regia ($2 \text{ HCl}:2\text{H}_2\text{O}:1 \text{ NHO}_3$). The etch was terminated by quenching with deionized water.

The ohmic contact formation is conducted in steps 4 and 5 of Figure 2. In step 4, a closely spaced (0.0005 inch) evaporation mask which defines the detector active area is placed in contact with the p-face of the crystal material resting in a holder. The entire fixture is then placed in a vacuum chamber


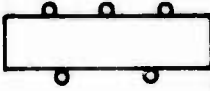


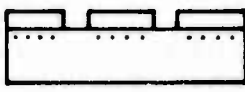
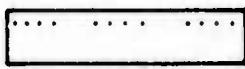


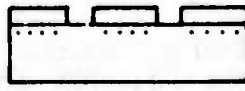
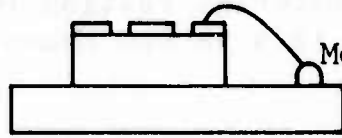
1.  Solution grown Cu-doped Gallium Phosphide
2.  Mechanical preparation of surface
3.  Chemical etch to eliminate surface damage
4.  Te-Ag-Ni contact evaporation through proper mask
5.  Sinter alloy into GaP
6.  Excess metal removed
7.  Applied photo resist (on the active area)
8.  Indium bonding pad evaporated
9.  Photo resist removed
10.  Mounted on package and TC bonded

Figure 2 GaP PHOTOCONDUCTIVE DETECTOR FABRICATION PROCEDURE

and a high vacuum ($< 2 \times 10^{-6}$ torr) established. The electrode alloy is then deposited by evaporation from a source held about 6 inches from the evaporation fixture. Two evaporation sources are used for each evaporation. The first is a molybdenum boat containing Ag-1% Te alloy source. The second is a tungsten boat containing nickel wire. Approximately 4 Å to 6 Å of tellurium is first evaporated and then the temperature of the molybdenum boat is increased to permit the evaporation of silver, about 600 Å. At this point, power to the boat is turned off. Nickel is then evaporated from the second evaporation. About 600 Å of nickel are evaporated.

Sintering of the evaporated alloy, step 5, was also carried out in a vacuum. The detectors are located next to a thermocouple placed in an aluminum oxide coated molybdenum boat. The condition adopted for successive sintering was to increase the boat temperature (thermal couple reading) to 520°C in 30 minutes, and to maintain it at 520°C for 20 minutes. After sintering, any excess metallic contaminant ions in the inter-electrode area are removed. In step 7, the active area is then covered by a protective coating by using a light field photomask and Shipley photoresist. A layer of indium (1/2 to 1 μm) is evaporated over the contact regions as shown in step 8 of Figure 2. In steps 9 and 10, the photoresist is removed and a 1-mil gold wire is thermal compression bonded to the In bonding pad. Finally, the device is attached with temporary adhesive to a flat pack and the gold wires are bonded to the terminals of the board. The device is ready for test.

2.2.2 Detector Preselection and Testing Procedures

During the star sensor and environmental testing programs, we followed the testing schedule shown in Figure 3. After Ag-1% Te and Ni contact evaporation and sintering, the detector is probed. Only if the sample shows light sensitivity under a microscope lamp, is the indium bonding pad then evaporated and the finished device mounted on the package for further testing. The dark current-voltage measurement is the first testing procedure to check if an ohmic contact has been achieved. The device is then tested for its spot scan response using a GFE star transit simulator. If the measured sensitivity of the device falls within a specified range of the design goal, then the detector optimum bias point, rise and fall time, and wideband noise are measured. Spectral responses of selected devices of each fabrication run are taken. After the device is fully characterized, it is ready for environmental test. Thirty-five

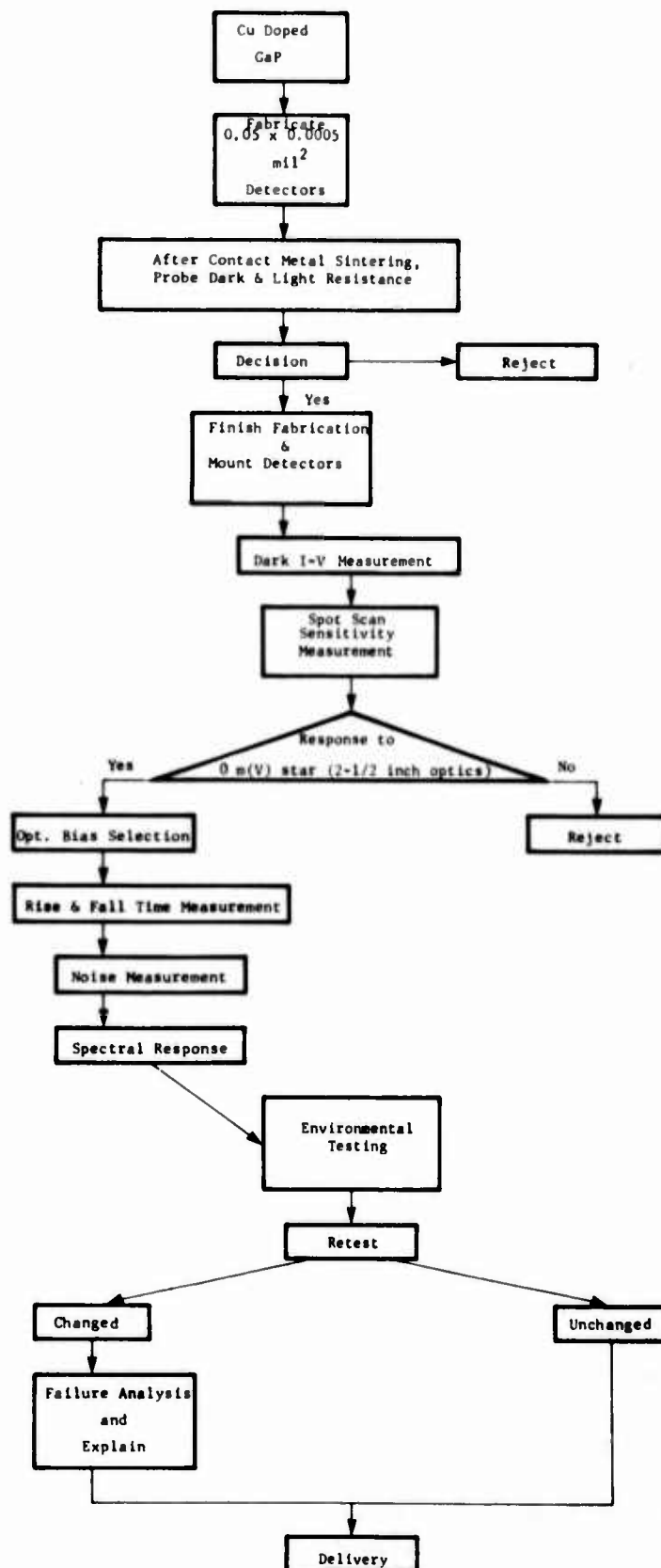


Figure 3 GaP SLIT DETECTOR TESTING PROCEDURE

selected slit detectors separately underwent the following tests: temperature cycle (4 detectors), humidity (5 detectors), vibration (4 detectors), solar exposure (5 detectors), thermal vacuum (8 detectors), electron irradiation (3 detectors), proton irradiation (3 detectors), gamma rays (3 detectors). Detectors were checked for sensitivity, noise, and rise and fall times after each environmental exposure. Any change or failure which occurred during the environmental testing was reported. The cause of failure was studied and corrective action was initiated to prevent reoccurrence of such a failure. The 35 detectors were then delivered to AFAL.

2.3 DETECTOR CHARACTERIZATION

The following methods were used to characterize the performance of the Cu-doped GaP slit detectors:

- Dark I-V measurement
- Spot scan sensitivity
- Noise measurement
- Rise and fall time
- Spectral response

2.3.1 Dark Current-Voltage Measurement

The current-voltage relation of each detector was measured with a Keithley electrometer. A battery bias voltage source, with a potentiometer, was used to set the bias voltage. Most detectors exhibited close to a perfect ohmic relationship. Typical examples are shown in Figures 4 and 5.

2.3.2 Spot Scan Sensitivity

The spot scan results were measured with a GFE star transit simulator. The source used was a 9-amp GE ribbon filament lamp operated from a controlled power supply. A0 spectral filters (BG 34-3.5 mm, KG 2-3.0 mm) and a set of neutral density filters could be inserted into it to simulate the desired color temperature and appropriate stellar magnitude. A small circular aperture was inserted into the optic path before the image lens. The image was a 1.5-mil diameter dot. The focus was adjusted to achieve maximum signal. A calibrated IL selenium detector (0.25 μm to 0.7 μm), an IL radiometer and a calibrated EG&G Si detector (0.4-1.0 μm) were used to calibrate the laboratory source. When

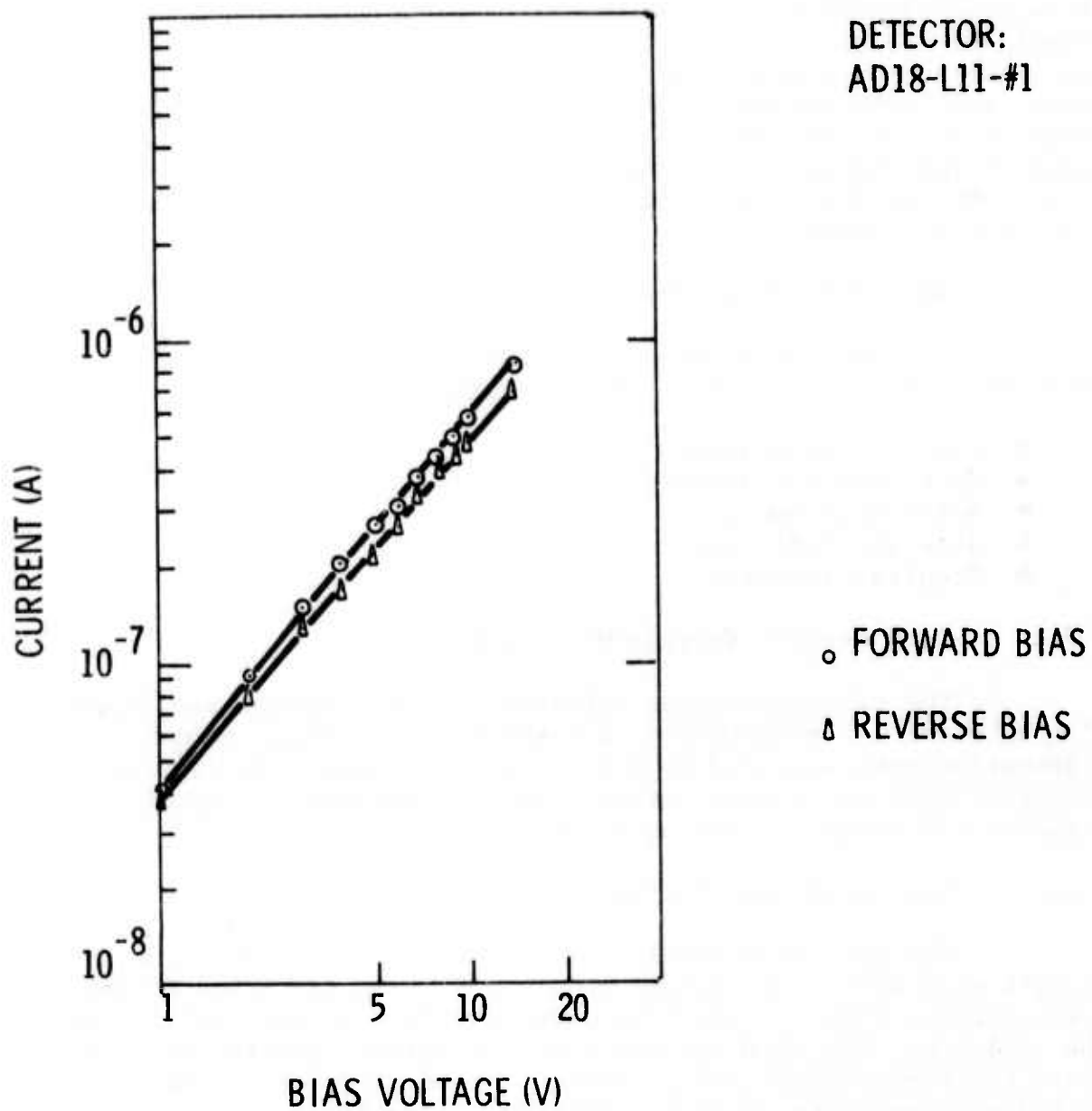


Figure 4 CURRENT VS APPLIED VOLTAGE OF A GaP PC SLIT DETECTOR

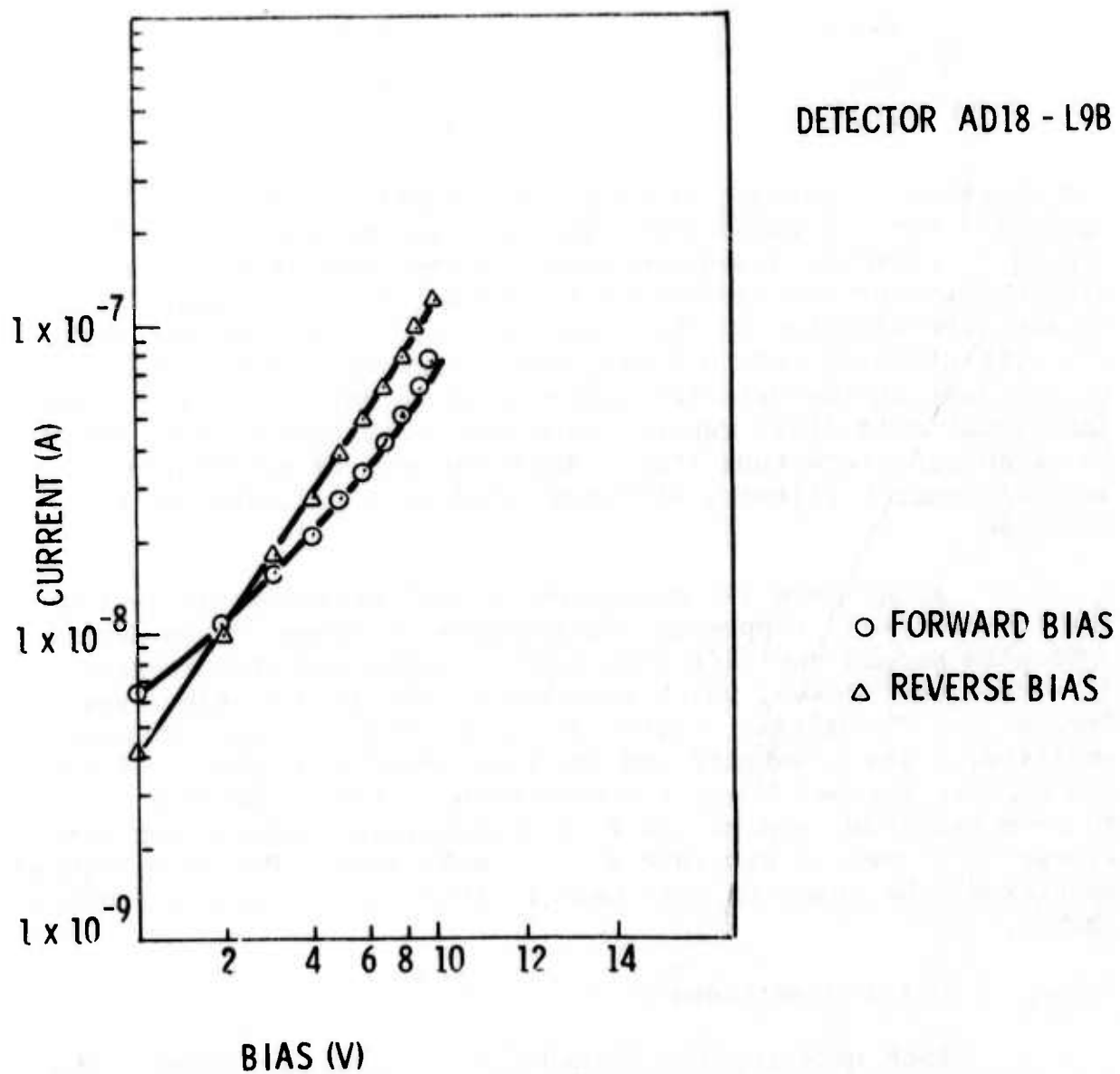


Figure 5 CURRENT VS APPLIED VOLTAGE OF A GaP PC SLIT DETECTOR

there is 8-amp current on the 9-amp lamp with BG and KG filters inserted, and ND filter setting at 53, the spectral irradiance of the source is:

Wavelength (nm)	Spectral Irradiance (W/nm)
399.5	2.5×10^{-13}
489.2	4.3×10^{-13}
549	2.9×10^{-13}
599	2.3×10^{-13}

The spectral irradiance of an A0 zero magnitude star (2-1/2 clear aperture) and the laboratory simulated source are plotted in Figure 6. The total optical power of the simulated source between 400 and 500 nanometers is about 1.5×10^{-11} watts. Because the diameter of the image spot is 1.5 mil and the detector slit width is only 0.5 mil, the actual optic power which is incident on the detector active area is only 8.6×10^{-12} watts. Throughout this final report, this test condition will be referred to as A0 zero magnitude star. With the aid of calibrated neutral density filters, different stellar magnitudes can be obtained.

After dark I-V measurement, each detector was tested for its spot scan response. Photographs of scope traces during spot scan across the slit from left to right and then reverse direction were taken, which resulted in two signal peaks (see Figure 7). The signal output was taken from a transimpedance amplifier. The schematic and the gain profile of the amplifier are shown in Figures 8 and 9 respectively. The calibrated A0 zero magnitude source and 0.1% transmission neutral density filter were used to simulate a +7.5 m(V) star. Unless otherwise specified, the scanning rate used in this test is always 0.00075 inch/s.

2.3.3 Noise Measurements

Each detector was tested for its wideband noise. The sequence is as follows. Connect detector noise output through the transimpedance amplifier (shown in Figure 8). Display the output on a storage oscilloscope with the time base set for 1 to 2 ms/cm with the trace free running. After about 5 seconds,

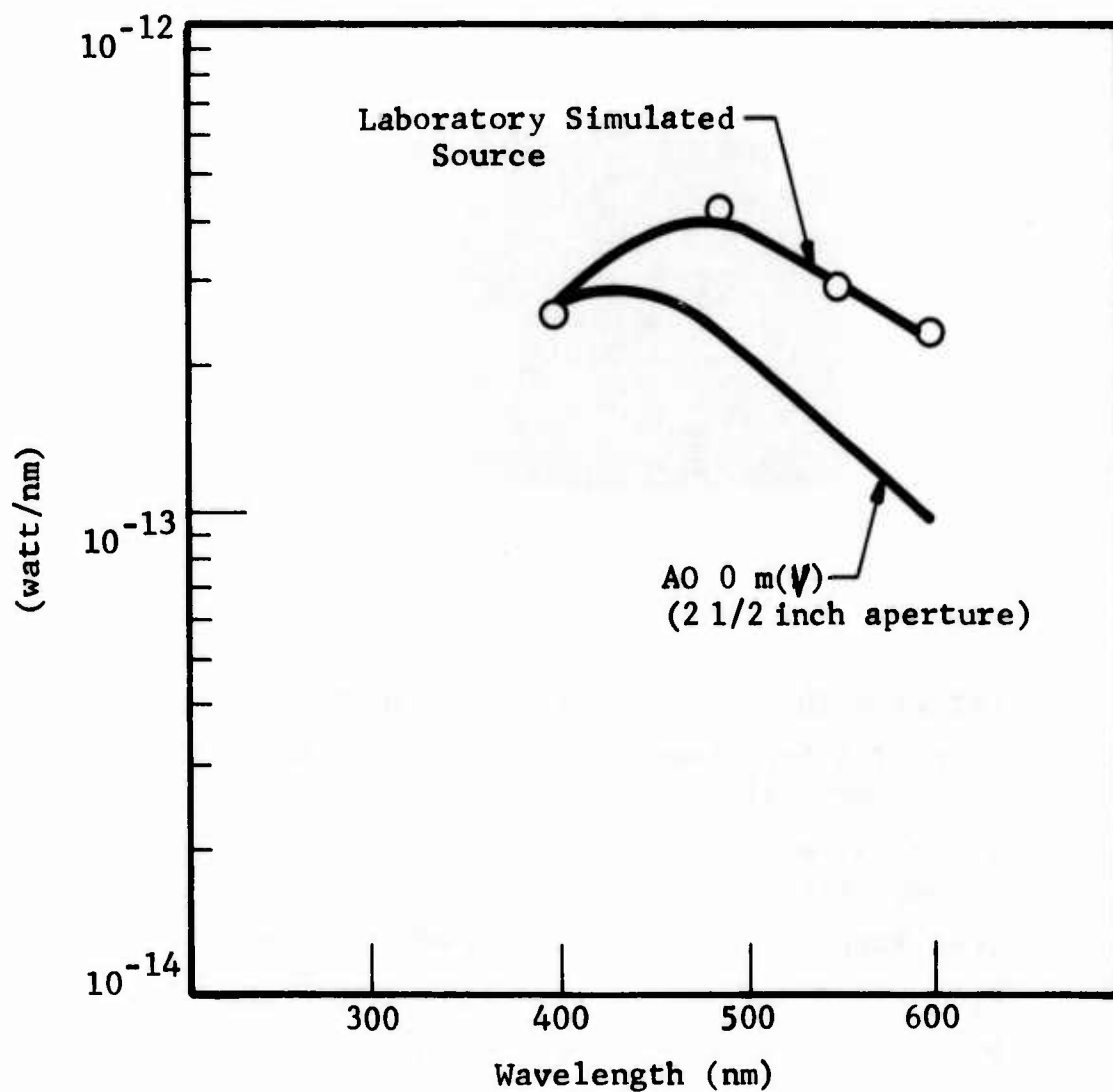
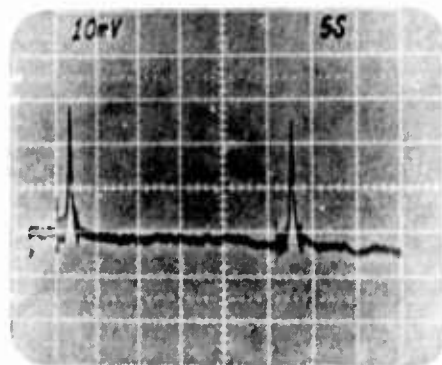


Figure 6 COMPARISON OF SPECTRAL IRRADIANCE OF AO CLASS STAR VEGA AND A LABORATORY SIMULATED SOURCE



Detector ID	=	AD25 M7 NO. 1
Star (2.5 in. clear aperture)	=	+7.5 m(V) AO
Signal after amplifier	=	28 mV
Scan Rate	=	0.00075 in./s
R_F	=	2.35×10^{10} ohm
V_B	=	-15 V

Figure 7 SPOT SCAN SENSITIVITY

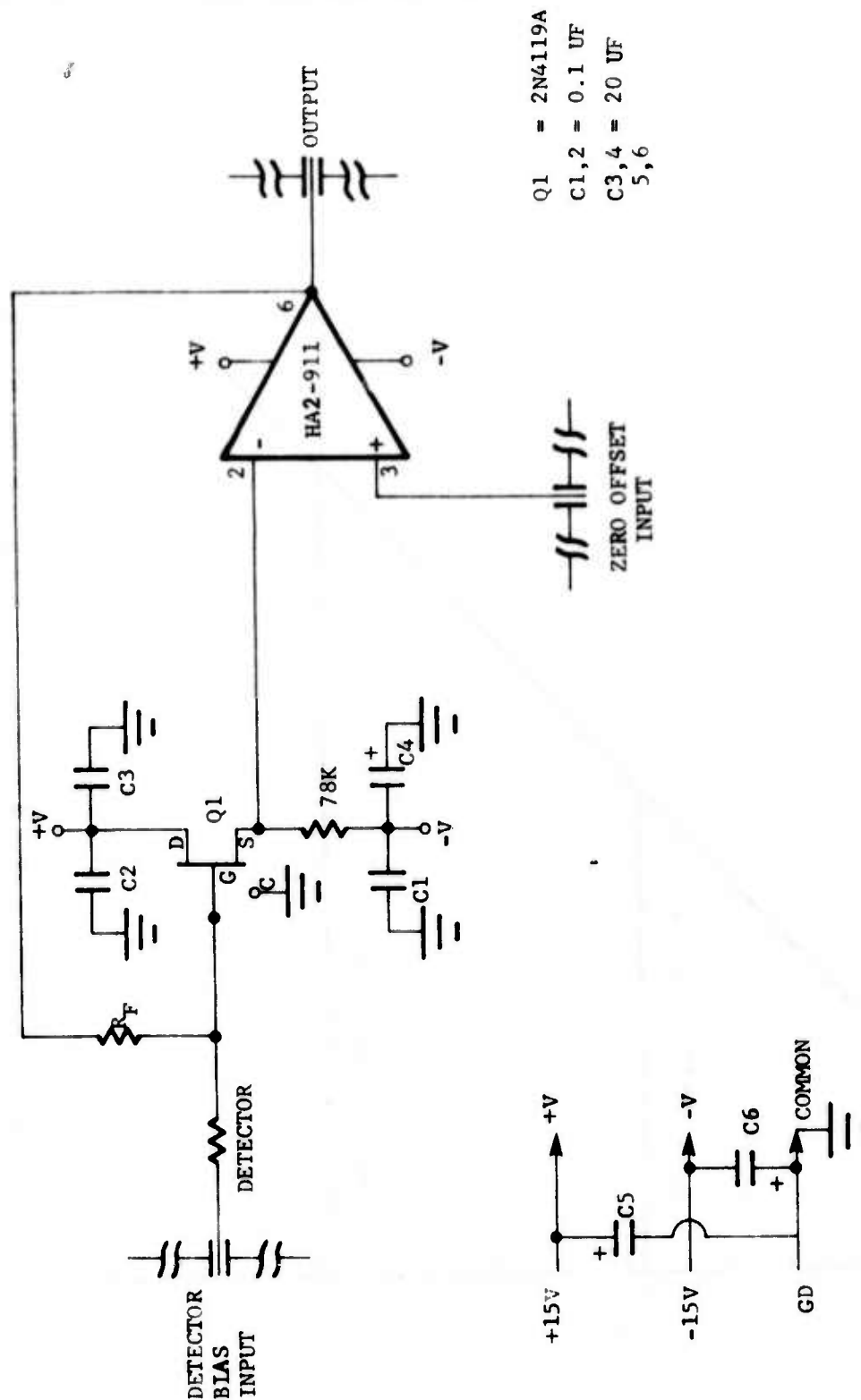
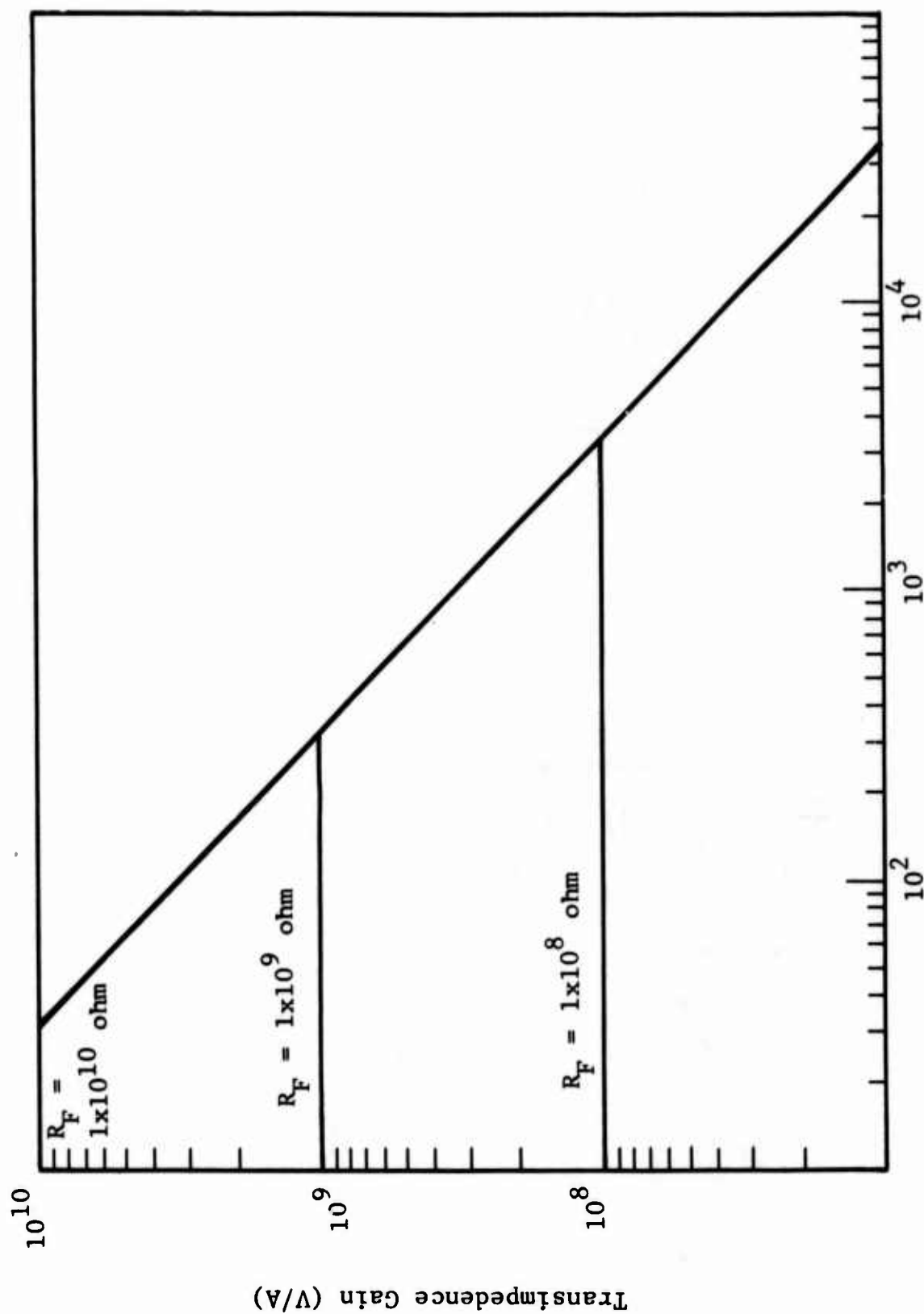


Figure 8 GaP PREAMPLIFIER



Frequency Response Character

Figure 9 SYSTEM GAIN PROFILE

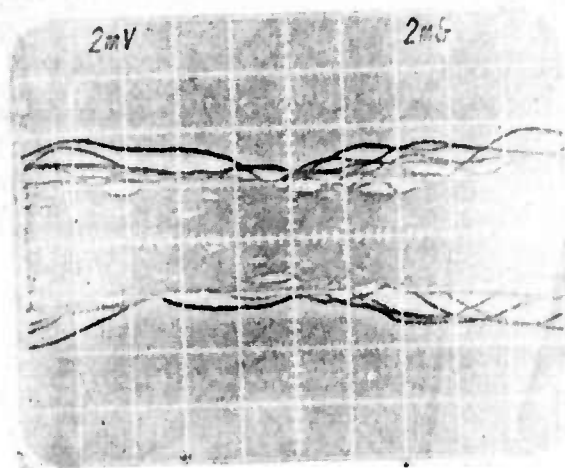
photograph the noise envelope with appropriate shutter speed. The photo will show the noise envelope during the storage period. Peak-to-peak noise voltage, V_N , pk-pk is taken to be the voltage difference between the extreme positive and negative deflection of the noise envelope. A sample of wideband noise of the slit detectors is shown in Figure 10.

The noise spectra of selected detectors were taken through the same amplifier circuit. We found that $1/f$ noise is a dominant noise source in most devices (see Figures 11 and 12). Surface recombination may be the origin of the excess $1/f$ noise in those slit detectors. The existence of depletion and inversion layers caused by interface states is the other possible explanation for the noise. Further investigation is required to understand and then to eliminate the excess noise.

2.3.4 Rise and Fall Time

A mechanical shutter was placed in the optical path of the spot scan setup. The spot was positioned on the detector active area. The rise time of the detector was obtained by opening the shutter and then measuring the time from the 10% to 90% point of the saturated dc shift of the output signal when the detector was dark and under illumination. Then the shutter was closed and again the fall time from the 10% to 90% point was taken. We observe, in general, there are two distinct rise times of the Cu-doped slit detector (see Figure 13): one very fast signal rise to the flat signal level plus a very slow rise to the saturated peak signal level. The observed slow response is caused by the gradual filling of the majority traps⁽⁵⁾. On the same figure the device has two distinct fall times; an initial fast fall time due to the recombination mechanism, followed by a long decay resulting from thermal emptying of the traps.

The photoresponse of the GaP:Cu sample to pulsed radiation was measured by Honeywell and AFAL. In Figure 14, the signal level varies as a 100-ms light pulse is repeated on the detector in 10 second intervals. Prior to the first pulse the detector had been stored in total darkness for 85 hours. At room temperature, all the majority traps are empty. During the first pulse, part of the photon generated electrons from the valence band are captured by the electron traps which yield a smaller signal pulse. The effect of majority traps is apparent, as evidenced by the increase of the height of the second pulse over the first.



Detector ID = AD18 M7 NO. 4
 $V_{Np.p}$ = 4 mV
 R_F = 2.3×10^{10} ohm
 V_B = -10 V

Figure 10 DETECTOR WIDEBAND NOISE

Detector AD18 MIA - #2
 $R_L = 2.3 \times 10^{10} \text{ ohm}$
 $V_{\text{bias}} = +20V$

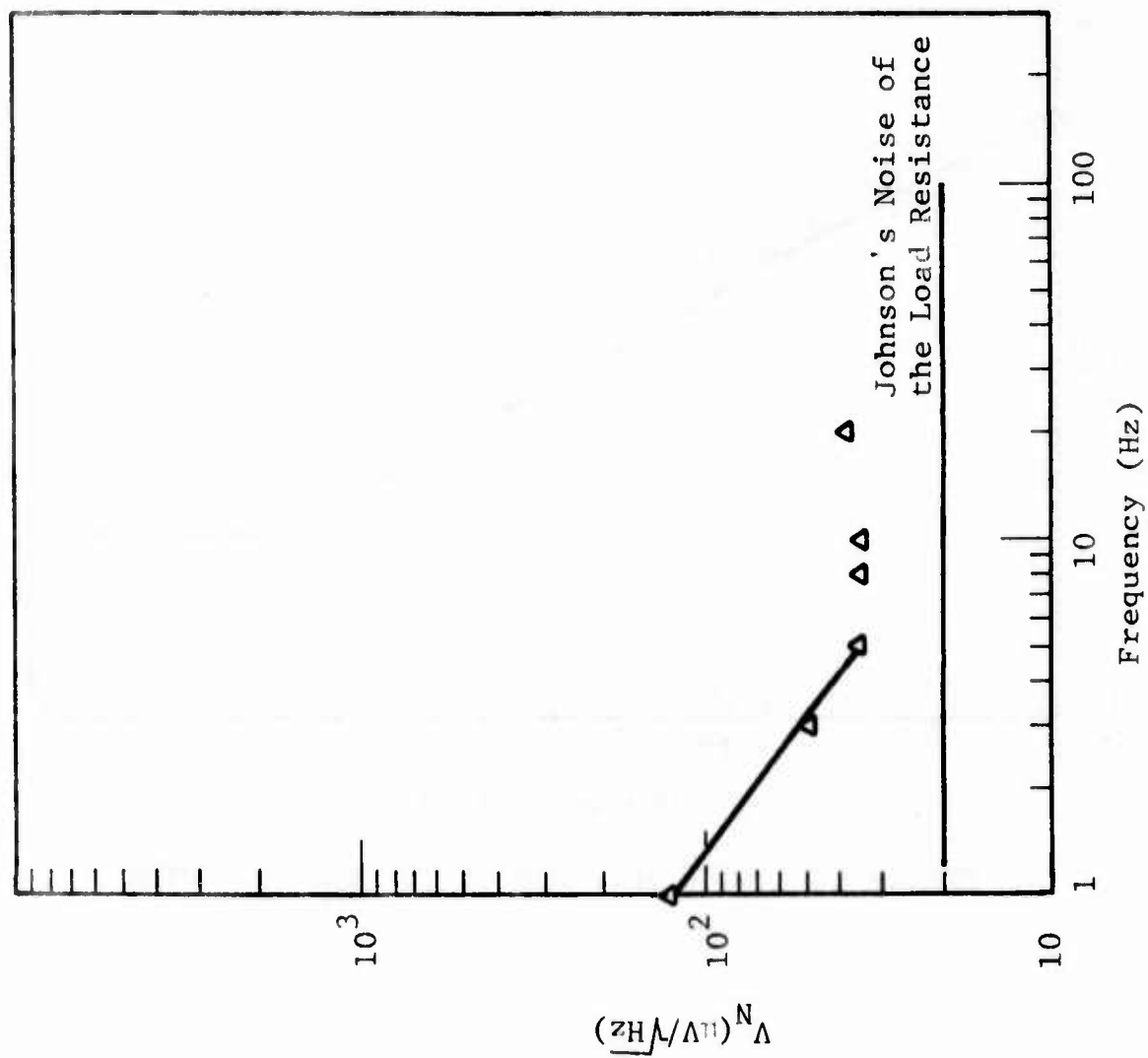


Figure 11 NOISE SPECTRA OF THE SLIT DETECTOR

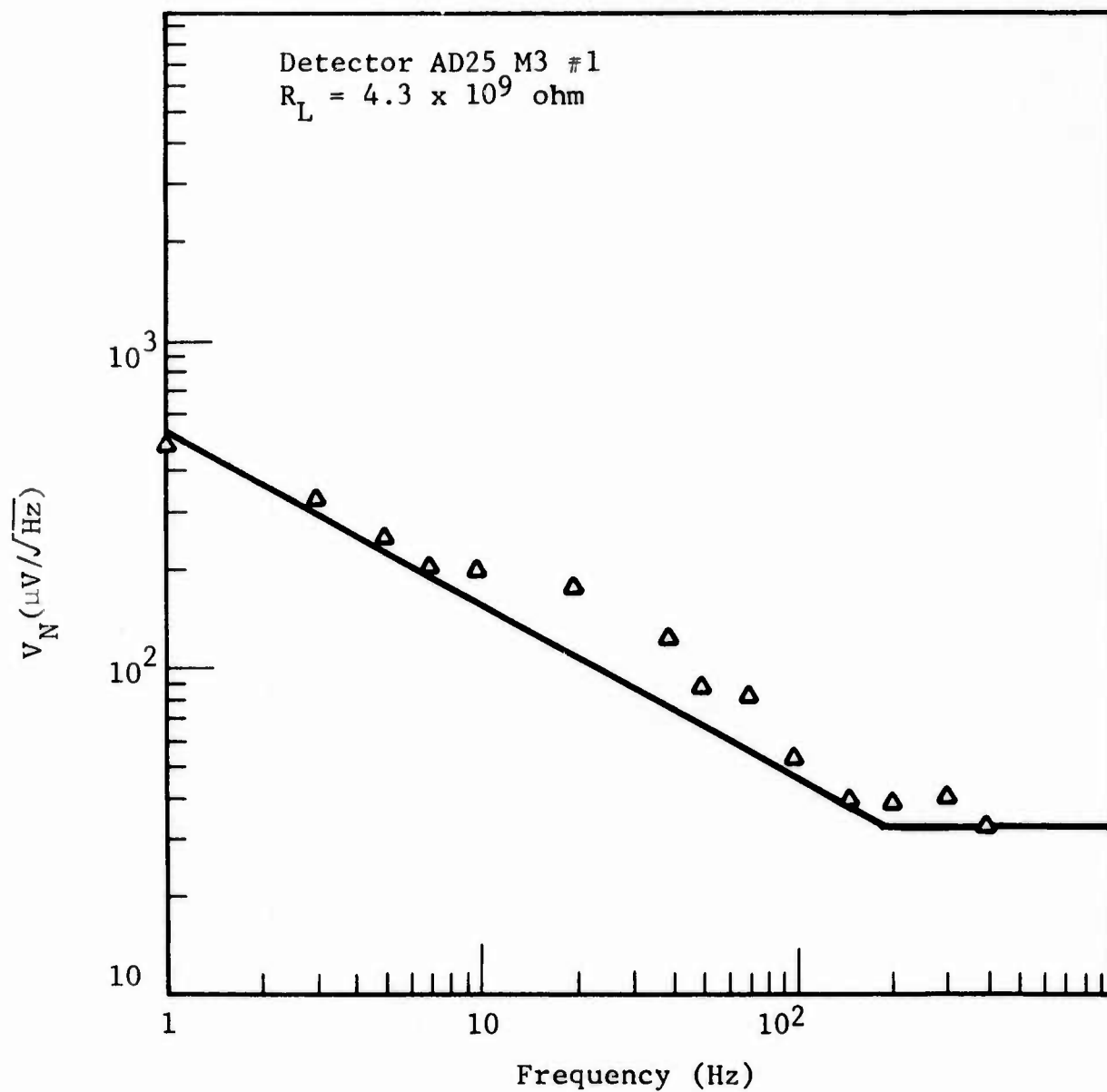
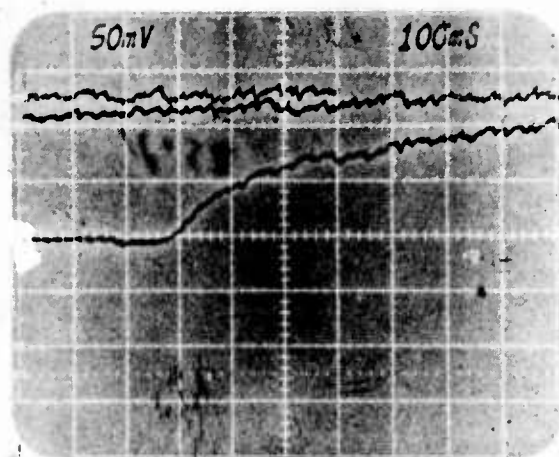
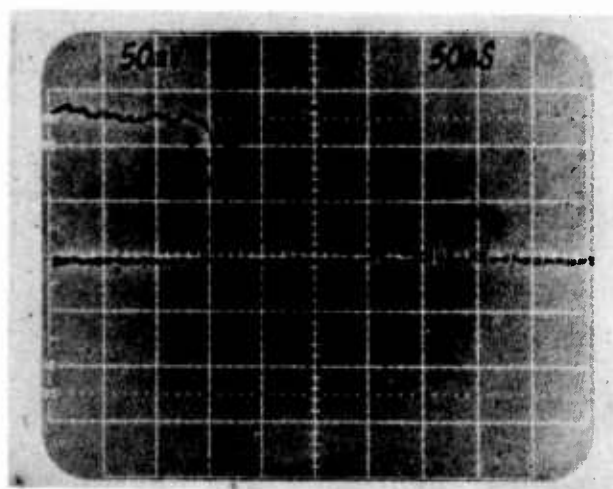


Figure 12 NOISE SPECTRUM OF THE SLIT DETECTOR



Rise Time



Fall Time

Detector ID = AD18 M7 NO. 8
 V_{BIAS} = -10 V
 R_F = 2.35×10^8 ohm
 Source = +2.5 m(V) (AO + 10% ND Filter)

Figure 13 DETECTOR RISE AND FALL TIME

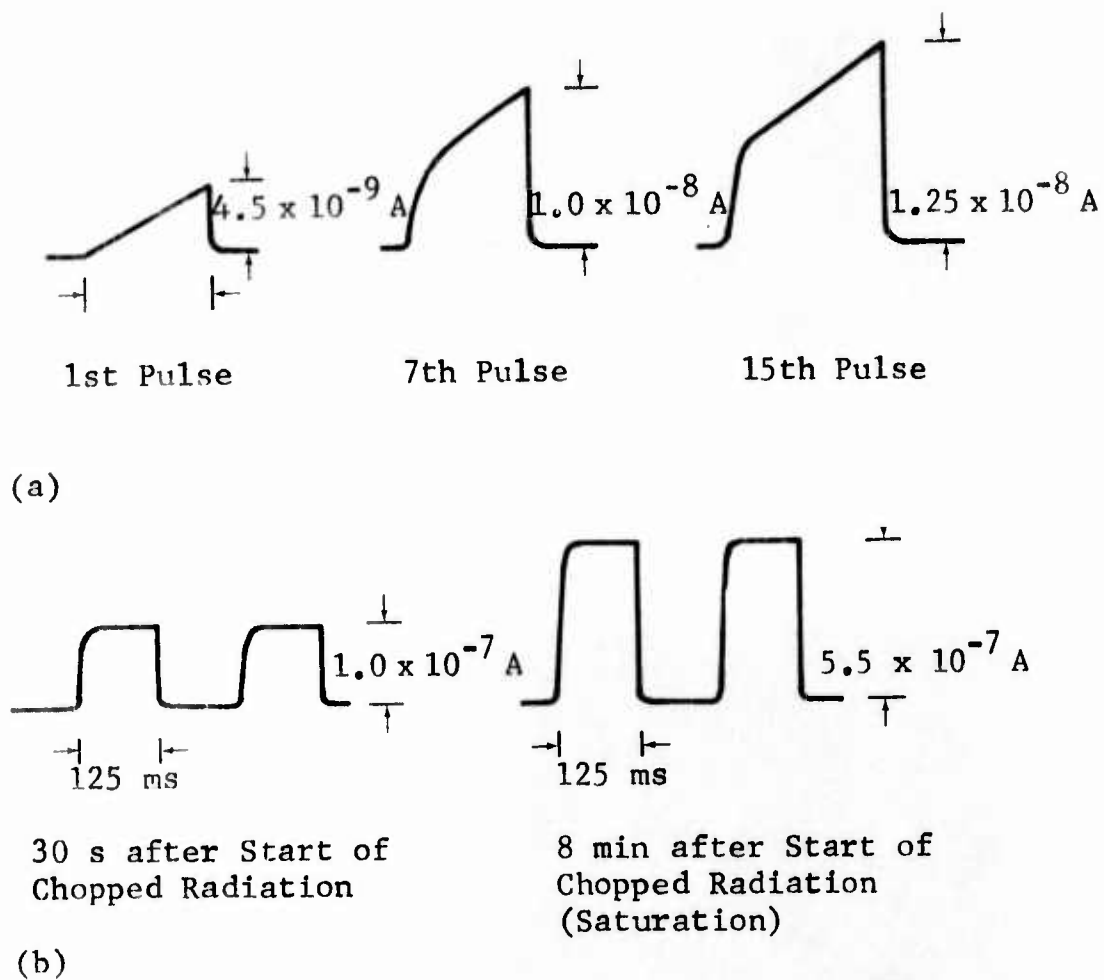


Figure 14 (a) TIME-DEPENDENT RESPONSE OF A GaP:Cu SAMPLE TO A SERIES OF 100-ms PULSES AT 10-s INTERVALS OF 2.8-eV RADIATION. (b) RESPONSE OF THE SAME SAMPLE TO A REGULARLY MODULATED SOURCE.

Pulse response data of the Cu-doped GaP slit detector were taken at AFAL and shown in Figure 15. As compared to Figure 14, the height of the pulse response is slowly decreasing to a steady value. This may be due to the presence of deep lying acceptor levels, which have a large cross section with respect to holes. The detector had been stored in the dark for 12 hours; all the levels are ionized (contain no holes) in the dark. The free holes created during the first pulse are captured by the empty acceptor levels which lead to a longer electron lifetime and higher signals. After the first pulsed excitation, because of the high binding energy of those levels, part of the captured holes will stay in these levels. During the second pulse, because part of the hole traps are already occupied, more free holes are produced in the valence band. The net effect of those free holes is an increase in electron recombination and yields a decrease in pulse height.

2.3.5 Spectral Response

The spectral response of the selected slit detectors was measured by using a tungsten source and a Jarrel Ash 0.25 meter Ebert monochrometer. The peak response of those detectors is around $0.5 \mu\text{m}$, as shown in Figures 16, 17 and 18. Because of the high absorption coefficient ($\alpha > 10^4 \text{cm}^{-1}$)⁽⁶⁾ of GaP at photon energies greater than 3 eV, the fast decrease of the spectral response at shorter wavelengths ($\lambda > 0.4 \mu\text{m}$) is indicative of high surface recombination. An improvement in surface preparation during the fabrication process is needed to give better response of high energy photons.

2.3.6 Photoconductive Gain Measurement

The photoconductive gain is defined as the ratio of the number of charge carriers passing through the external circuit per second to the number of photons incident on the detectors per second. The photoconductive gain was obtained by measuring the dc shift of the output signal both when the slit detector is dark and under the illumination of a 1.5-mil dot. A sample calculation is shown as follows:

Detector: AD18M1A No. 2
 Incident flux: $1.7 \times 10^{-7} \text{ watts/cm}^2$ at $0.489 \mu\text{m}$
 Bias voltage: 20 V
 $R_F = 2.3 \times 10^{10} \text{ ohms}$
 Signal through amplifier = 250 mV
 $A = \text{slit area under illumination} = 4.85 \times 10^{-6} \text{cm}^2$

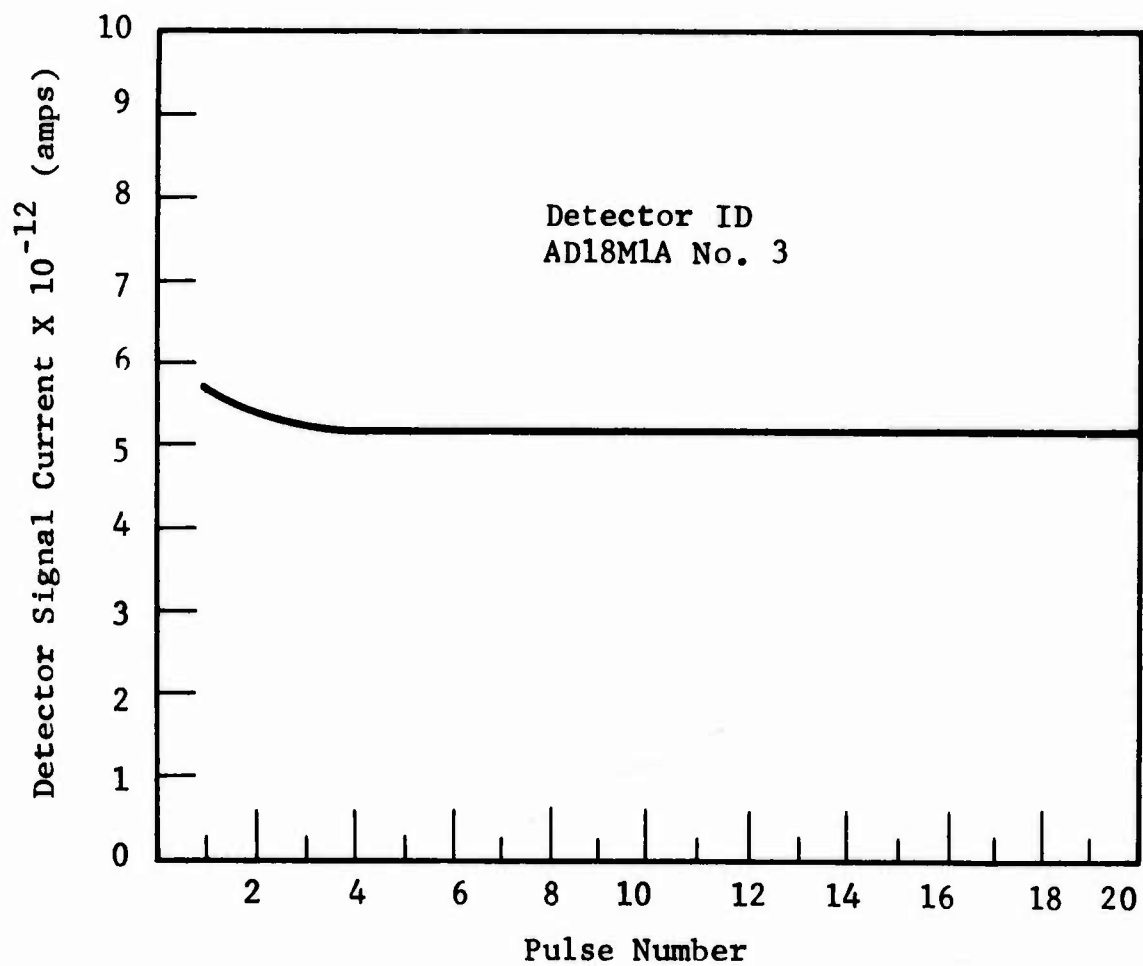


Figure 15 DETECTOR PULSE RESPONSE

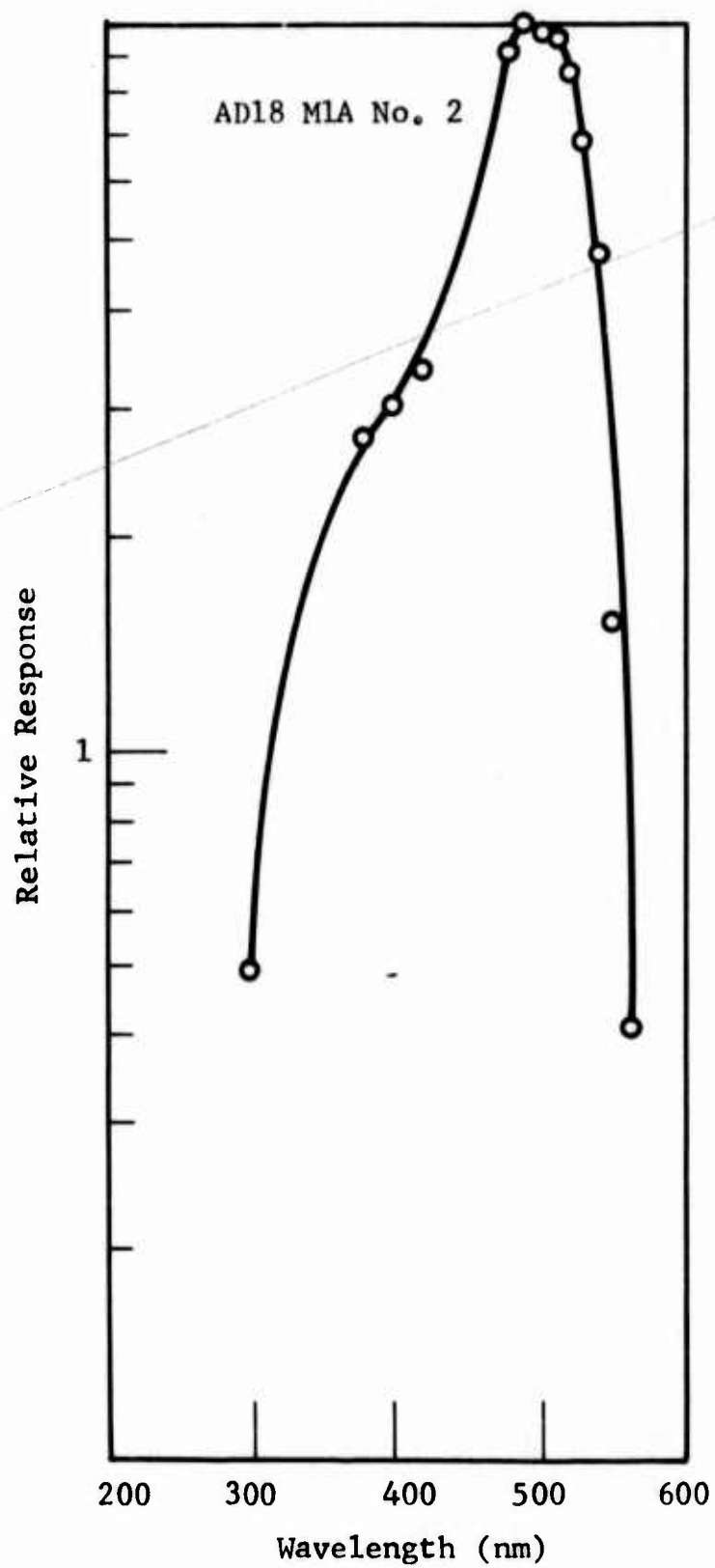


Figure 16 GaP PC SET DETECTOR RELATIVE SPECTRAL RESPONSE

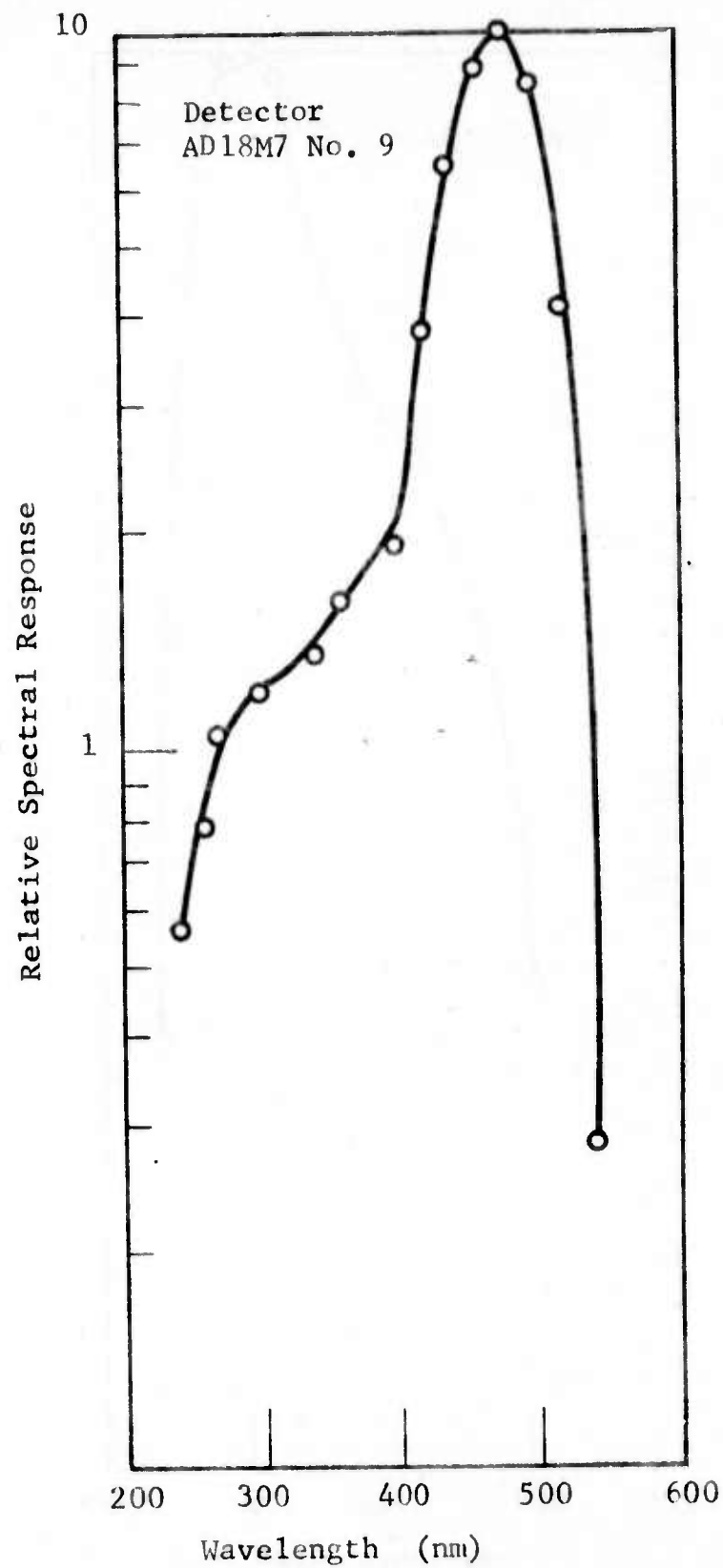


Figure 17 GaP PC SLIT DETECTOR RELATIVE SPECTRAL RESPONSE

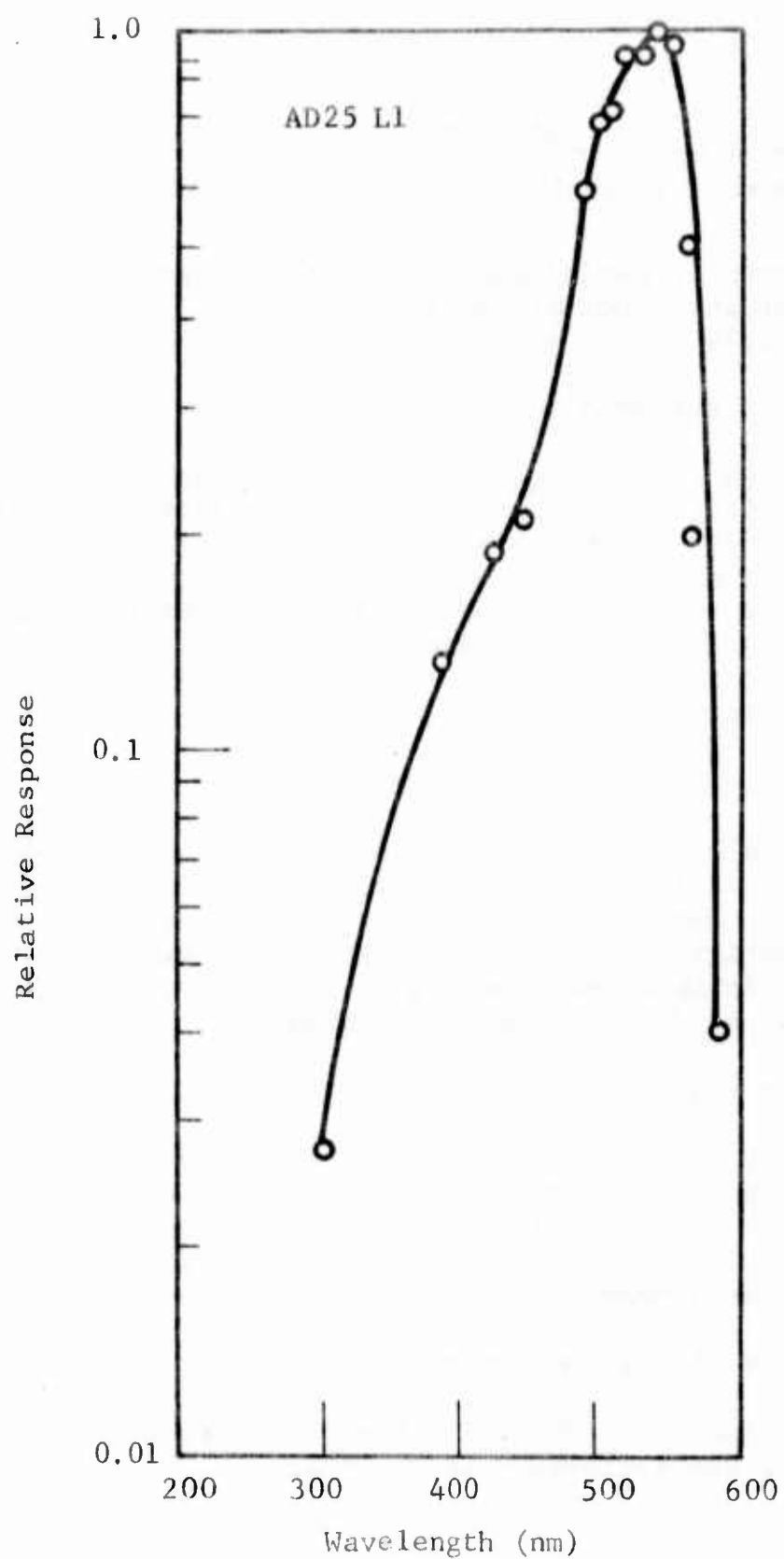


Figure 18 GaP PC SLIT DETECTORS RELATIVE SPECTRAL RESPONSE

$$\text{Gain} = \frac{260 \times 10^{-3}}{2.46 \times 10^{18} \times 1.7 \times 10^{-7} \times 4.86 \times 10^{-6} \times 2.3 \times 10^{10} \times 1.6 \times 10^{-19}} = 35$$

If the illumination is positioned in a different active area of the same detector, photoconductive gain as high as 300 has been observed. See Table 1.

2.3.7 Detector Uniformity

Spot scan response along the detector active area was measured. It indicates that lack of spot scan uniformity along the slit is the chief drawback of those devices (see Figures 19 and 20). As stated in the beginning of this report, for the photoconductive mode detector, very high purity, high resistivity, n-type material is required. Considerable material growth development effort is still required to achieve accurate compensation and uniformity.

2.3.8 Linearity of the Detector Response

Measurements of the dependence of spot scan response on the excitation energy were made. One can see in Figures 21 and 22, the response vs light intensity is linear in the energy range under investigation. Similar tests were taken by AFAL on five delivered slit detectors (see Figure 23). Over four orders of magnitude linear dynamic range was obtained.

2.3.9 Optimum Bias Point

The spot scan response and pk-pk noise data of each detector was measured under different bias conditions. An optimum bias point corresponding to the maximum signal and noise ratio was selected for each detector. A bias dependent signal and noise measurement is plotted in Figure 24.

2.4 DETECTOR PERFORMANCE SUMMARY SHEET

The performance of the 35 slit detectors before the environment tests are summarized in Table 2.

Table 1

DETECTOR AD18MLA No. 2 - $R_F = 2.3 \times 10^{10} \Omega$, $V_{bias} = 20V$, $P_{in} = 8.4 \times 10^{-13}$ watts,

SCANNING RATE = 0.75 mils/s

Scan No.	Spot Scan Sensitivity mV	Rise Time	Saturated dc Response mV	Photoconductive Gain (ηG)	Majority Carrier Lifetime* ns
1	20	100 ms	20	2.6	5.2
2	38	1.2 s	45	5.8	12
3	30	700 ms	30	3.9	8
4	32	7 s	175	22.6	48
5	50	1.5 s	80	10.4	20
6	20	100 ms	20	2.6	5.2
7	20	100 ms	20	2.6	5.2
Hot spot	1000	85	2500	323	650

* NOTE: Majority carrier lifetime is calculated from the saturated photocurrent assuming $\eta_u = 40$

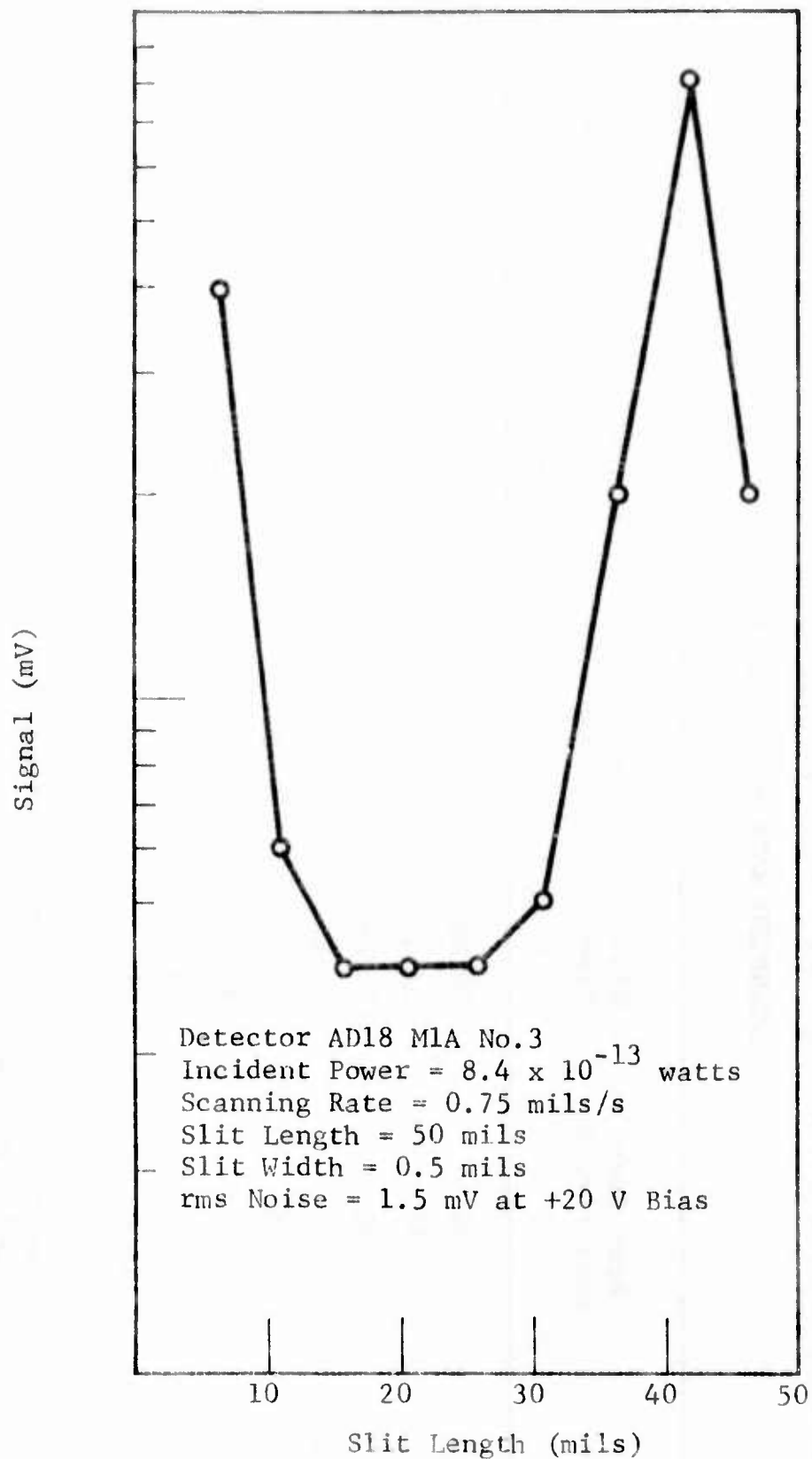


Figure 19 SPOT SCAN UNIFORMITY ALONG THE SLIT LENGTH

DETECTOR RESPONSE VS POSITION

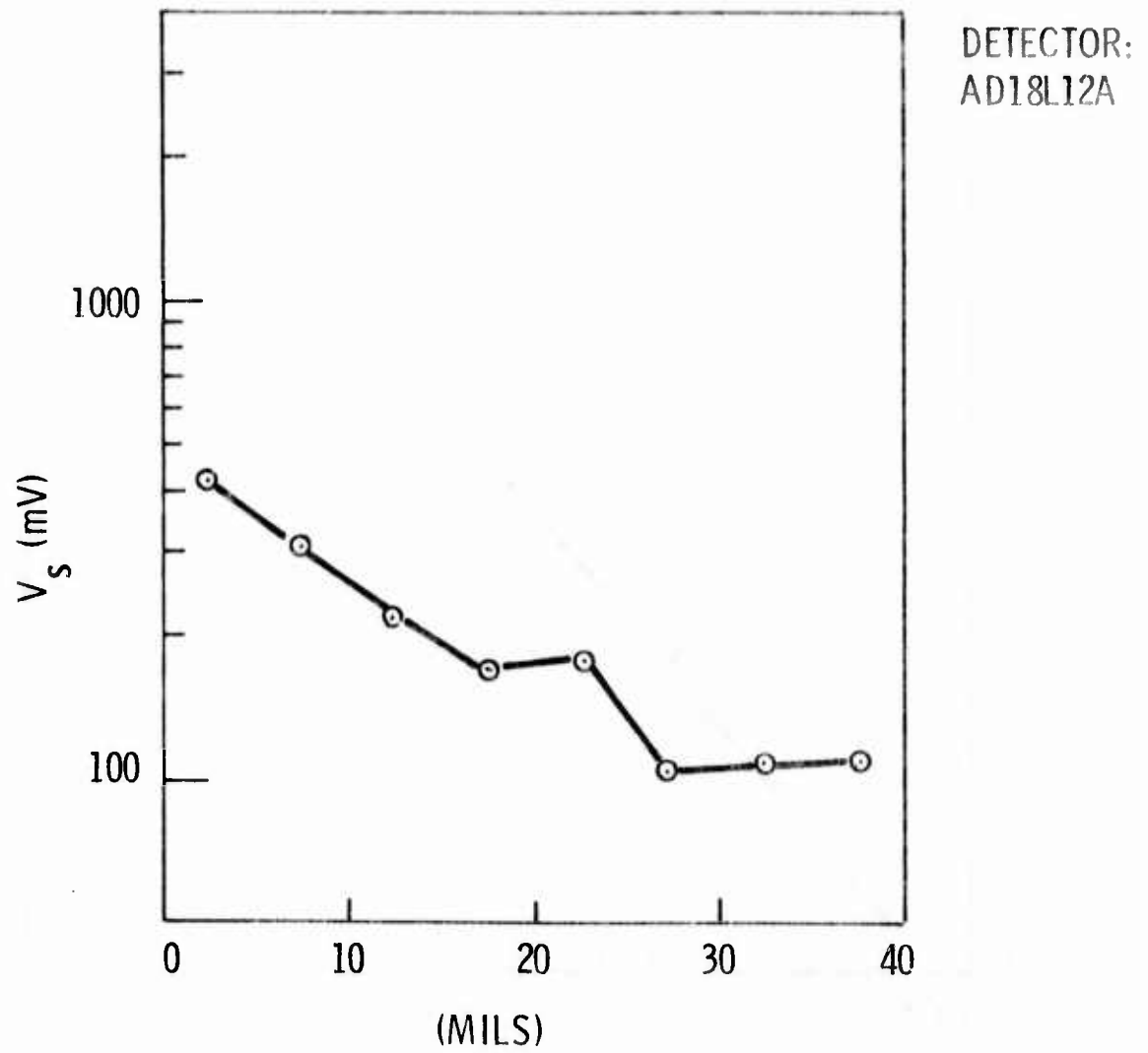


Figure 20 SPOT SCAN UNIFORMITY ALONG THE SLIT LENGTH

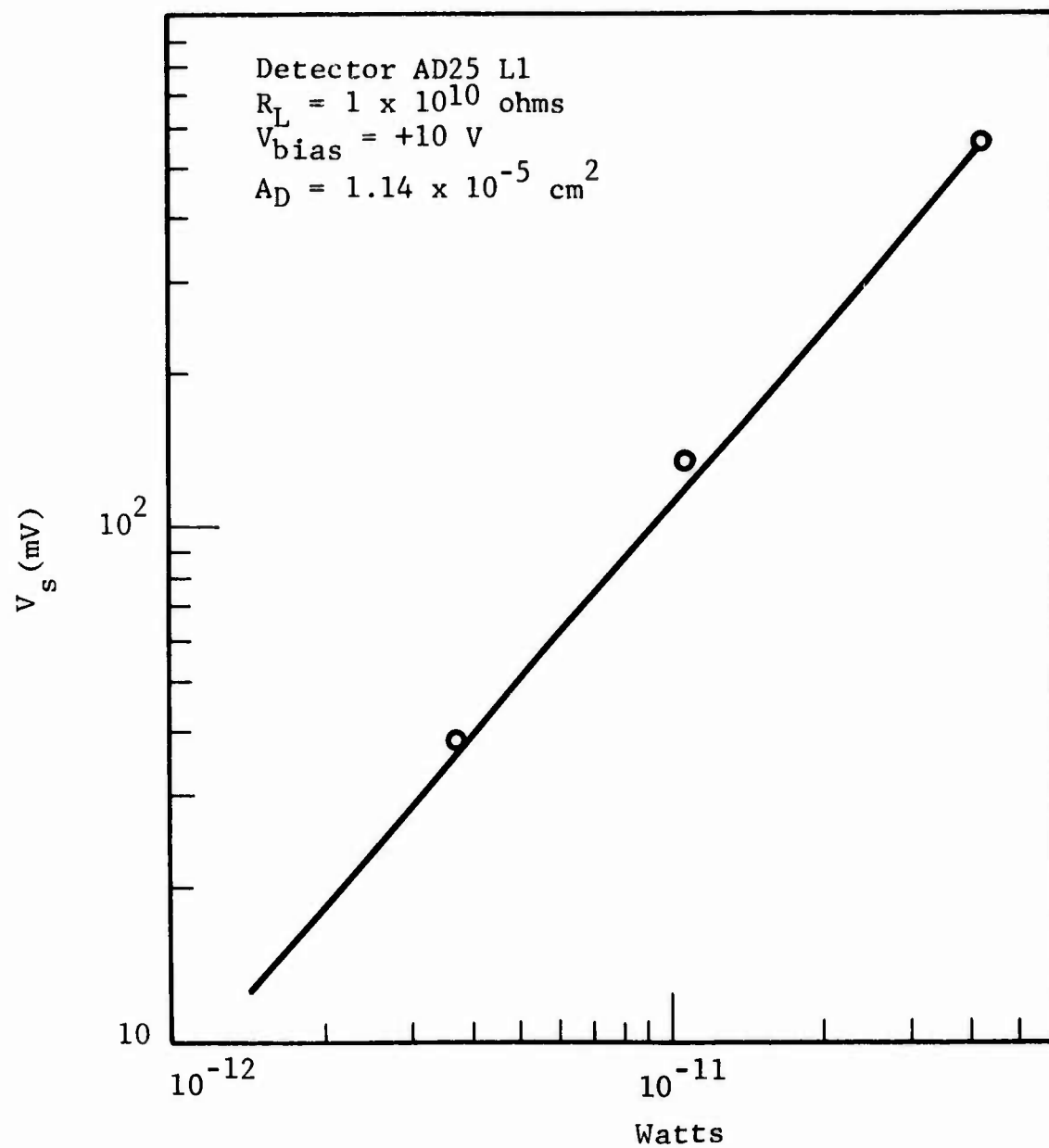


Figure 21 DETECTOR RESPONSE VS INPUT POWER

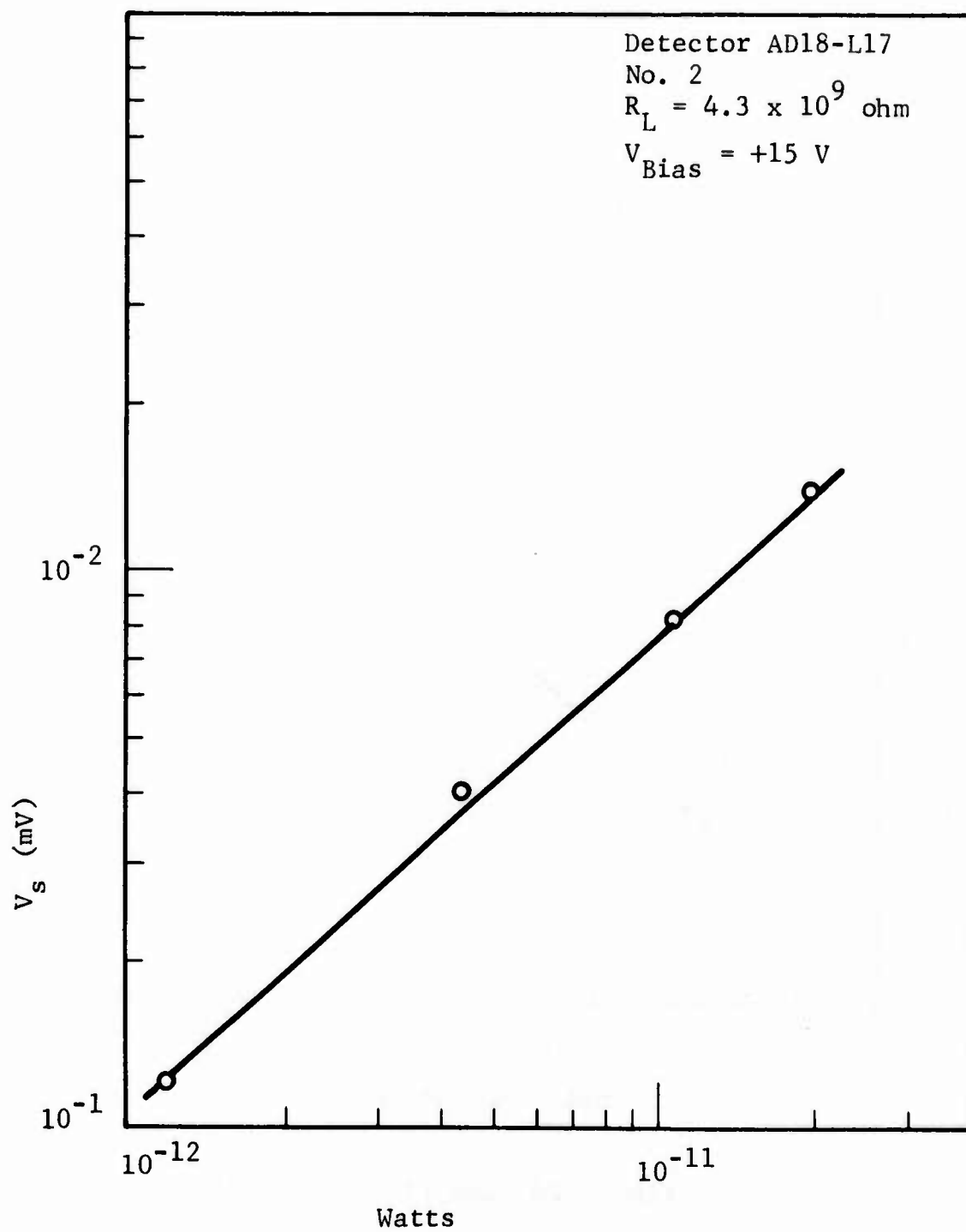


Figure 22 DETECTOR RESPONSE VS INPUT POWER

AFAL DATA

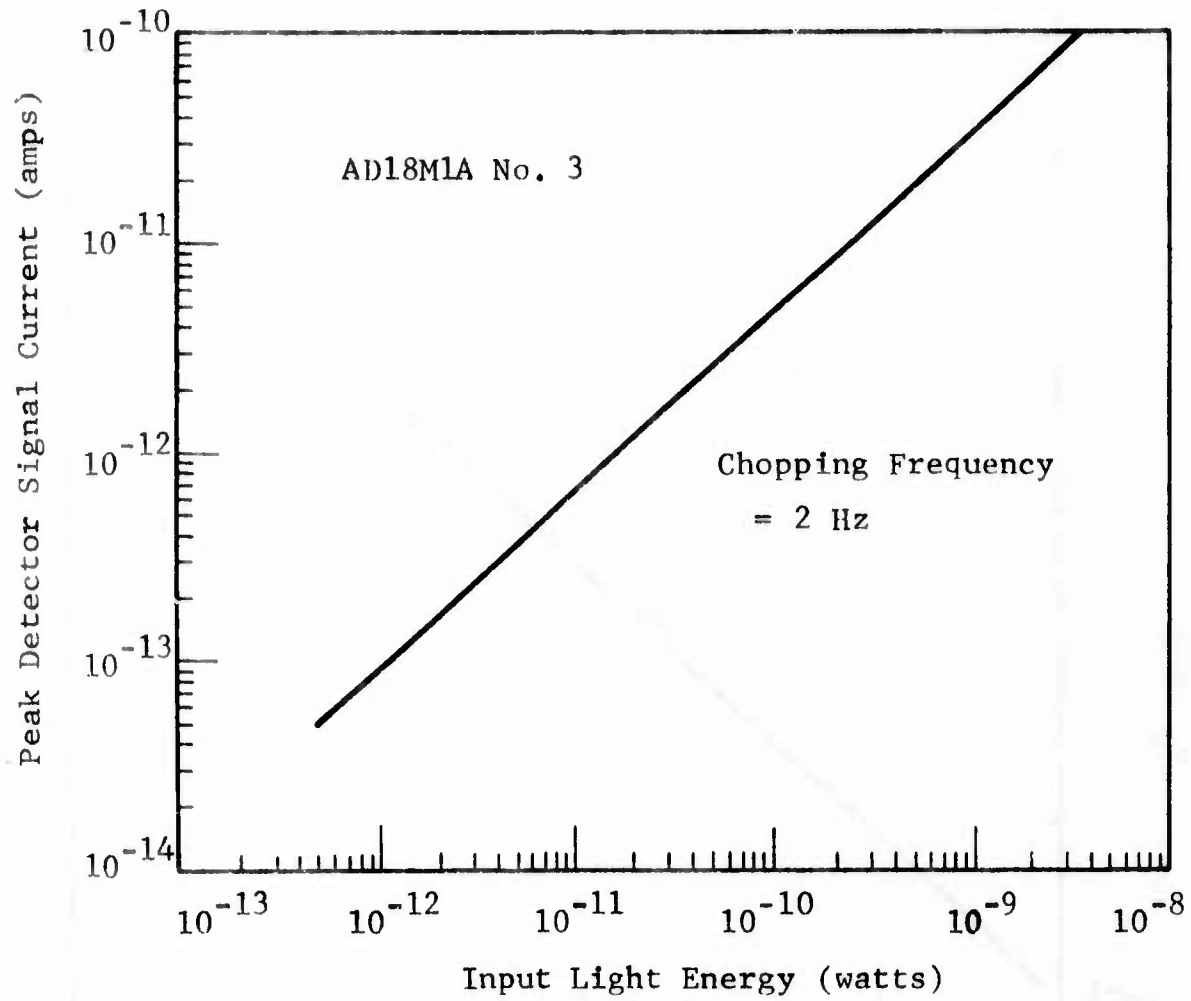


Figure 23 GaP LINEARITY DATA

Detector
AD18-L12A

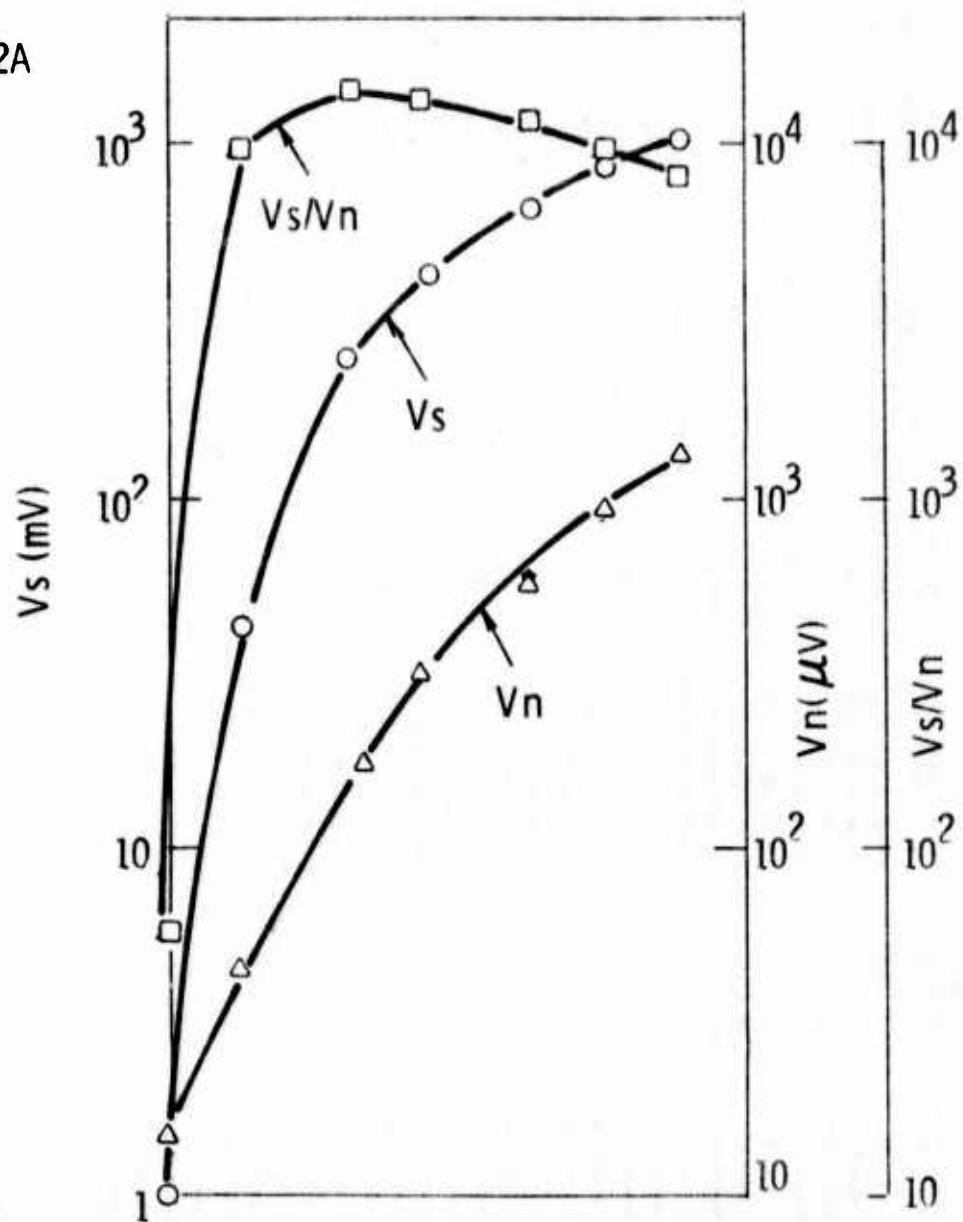


Figure 24 OPTIMUM BIAS POINT OF THE SLIT DETECTOR

Table 2
35 GaP SLIT DETECTORS PERFORMANCE SUMMARY CHART

Detector ID	Environmental Test	Dark Resistance (ohm)	Spot Scan Sensitivity	Noise V_N pk-pk	Optimum Bias	Rise Time	Fall Time	R_F (ohm)
AD18-L4 No. 1B	Electron	2.5×10^8	50 mV at 0 m(V)	600 μ V	-15 V	200 ms	100 ms	3×10^7
AD18-L5 No. 1	Temperature	1.1×10^9	70 mV at +2.5 m(V)	4 mV	-5 V	-	-	-
AD18-L6 No. 1	Temperature	7.7×10^7	14 mV at +2.5 m(V)	1 mV	-	-	-	-
AD18-L9 No. B	Gamma	1.4×10^8	40 mV at +2 m(V)	3.8 mV	+13.5 V	60 ms	-	3×10^7
AD18-L11 No. 2	Temperature	6×10^7	5.6 mV at 2.5 m(V)	-	-	-	-	-
AD18-L12 No. 1	Electron	1.8×10^9	30 mV at 0 m(V)	500 μ V	-5V	200 ms	50 ms	1×10^8
AD18-L16 No. 1	Humidity	4.6×10^8	120 mV at 0 m(V)	20 mV	+10 V	10 ms	80 ms	3×10^7
AD18-L16 No. 2	Humidity	4.7×10^8	60 mV at +0.75 m(V)	20 mV	+10 V	80 ms	80 ms	3×10^7
AD18-L17 No. 1	Gamma	4.2×10^{10}	25 mV at +2 m(V)	2 mV	-5 V	250 ms	400 ms	1×10^{10}
AD18-L17 No. 2	Gamma	1.4×10^{10}	120 mV at +2 m(V)	4 mV	+15 V	80 ms	80 ms	4×10^9
AD18-M7 No. 1	Thermal Vac	6.4×10^{11}	32 mV at +2.5 m(V)	4 mV	-7 V	170 ms	200 ms	2.3×10^{10}
AD18-M7 No. 2	Thermal Vac	3.0×10^{11}	120 mV at 0 m(V)	8 mV	-7 V	100 ms	90 ms	2.3×10^{10}
AD18-M7 No. 3	Thermal Vac	3.6×10^{11}	160 mV at +1.2 m(V)	6 mV	-10 V	120 ms	100 ms	2.3×10^{10}
AD18-M7 No. 4	Thermal Vac	2.5×10^{11}	38 mV at +2.5 m(V)	4 mV	-10 V	300 ms	300 ms	2.3×10^{10}
AD18-M7 No. 5	Proton	1.2×10^{11}	50 mV at +5 m(V)	5 mV	+5 V	50 ms	70 ms	2.3×10^{10}
AD18-M7 No. 6	Proton	2.3×10^{11}	80 mV at +1.2 m(V)	6 mV	+5 V	90 ms	150 ms	2.3×10^{10}
AD18-M7 No. 7	Proton	5.4×10^{11}	460 mV at +5 m(V)	6 mV	-7 V	2.2 s	120 ms	2.3×10^{10}
AD18-M7 No. 8	Thermal Vac	2.8×10^9	50 mV at +2.5 m(V)	6 mV	-10 V	800 ms	100 ms	2.3×10^8
AD18-M7 No. 9	Thermal Vac	7×10^{11}	600 mV at +5 m(V)	8 mV	+10 V	800 ms	200 ms	2.3×10^{10}
AD18-M8 No. 1	Solar	1.3×10^{10}	360 mV at +5 m(V)	30 mV	-10 V	1 s	300 ms	1×10^{10}
AD18-M8 No. 2	Solar	8.3×10^{10}	120 mV at +2.5 m(V)	18 mV	-16 V	1.2 s	200 ms	4.3×10^9
AD18-M8 No. 3	Solar	4.2×10^9	80 mV at 0 m(V)	18 mV	+10 V	500 ms	300 ms	9×10^8
AD18-M9 No. 4	Vibration	4.1×10^8	140 mV at +2.5 m(V)	5 mV	+15 V	40 ms	40 ms	3×10^7
AD18-M9 No. 6	Vibration	2.7×10^9	100 mV at m(V)	5 mV	+15 V	400 ms	100 ms	3×10^7
Cu9-L6	Temperature	1.4×10^7	10.5 mV at +2.5 m(V)	2.2 mV	-	-	-	-
AD24-L1 No. 1	Thermal Vac	1.9×10^6	-	-	-	-	-	-
AD24-L1 No. 4	Thermal Vac	5.3×10^6	-	-	-	-	-	-
AD25-M3 No. 1	Electron	4.0×10^9	2.5 V at +2.5 m(V)	3.2 mV	-6 V	100 ms	100 ms	2.3×10^8
AD25-M5 No. 1	Vibration	2.5×10^7	300 mV at +2.5 m(V)	5 mV	-10 V	800 ms	500 ms	-
AD25-M5 No. 2	Vibration	2.0×10^8	45 mV at +2.5 m(V)	2 mV	-5 V	800 ms	1.4 s	-
AD25-M6A No. 1	Humidity	1.0×10^{10}	700 mV at 1.2 m(V)	16 mV	-15 V	1.1 s	3 s	9×10^8
AD25-M6A No. 2	Humidity	3.9×10^{10}	400 mV at 0 m(V)	12 mV	+15 V	400 ms	1 s	9×10^8
AD25-M6A No. 5	Humidity	4.0×10^{10}	200 mV at +5 m(V)	5 mV	+5 V	250 ms	250 ms	1×10^{10}
AD25-M7 No. 1	Solar	2.0×10^{11}	30 mV at +7.5 m(V)	5 mV	-15 V	600 ms	260 ms	2.3×10^{10}
AD25-M7 No. 2	Solar	4.4×10^8	30 mV at +2.5 m(V)	6 mV	+15 V	400 ms	240 ms	3×10^7

SECTION III

ENVIRONMENTAL TEST RESULTS

Under AFAL Contract No. F33615-74-C-1121, 35 gallium phosphide photoconductive slit detectors fabricated from Cu-doped material were subjected to a series of environmental tests; temperature cycle, humidity, vibration, solar exposure, electron irradiation, proton irradiation and gamma ray exposure. Detectors were checked for sensitivity, noise, and rise and fall times before and after each environmental exposure. Any changes in detector performance were noted. The detailed test conditions are described below.

3.1 TEMPERATURE CYCLE

Four detectors were exposed to 0°F, 100°F, 200°F and 290°F for 10 hours each. One detector was capable of operating without degradation after each increment of temperature. The other three detectors passed at 200°F exposure. The indium bonding pads of the devices started to melt and shorted the active area at 290°F. GaP is a large bandgap semiconductor and is capable of operating at high temperature. GaP rectifier operating at 500°F has been reported⁽⁶⁾. For the purpose of higher device storage and operating temperature, a high melting point metal such as gold is recommended for use as a bonding pad.

The device performance before and after each temperature exposure is summarized in Table 3.

3.2 VIBRATION

Four detectors (AD18 M9 No. 4, AD18 M9 No. 6, AD25 M5 No. 1, and AD25 M5 No. 2) were capable of operating without degradation after exposure to the following vibration levels on each of the three mutually perpendicular axis

Frequency Range (Hz)	G-Level
10 - 14	2.5g
14 - 40	5.0g
40 - 400	15.0g
400 - 3000	25.0g

This test was performed at Air Force Cambridge Research Laboratories.

Table 3
TEMPERATURE CYCLE TEST RESULTS

Detector	Spot Scan Sensitivity [± 1.2 m(V)]			Noise			Dark Resistance Ω		
	Before	After 200°F	After 290°F	Before	After 0°F	After 200°F	After 290°F	After 200°F	After 290°F
AD18-L5	70 mV	70 mV	--(1)	4 mV	4 mV	4 mV	--(1)	1.1×10^9	--(1)
AD18-L6 No. 1	14 mV	14 mV	14 mV	1.2 mV	1.2 mV	1.2 mV	2.4 mV	7.7×10^7	7.7×10^7
AD18-L11 No. 2	5.6 mV	5.6 mV	--(2)	0.5 mV	0.6 mV	0.7 mV	--(2)	6×10^7	--(2)
Cu9-L6	10.5 mV	10.5 mV	--(1)	2.2 mV	2.2 mV	2.5 mV	--(1)	1.4×10^7	--(1)

NOTES: (1) Indium started to melt.

(2) TC bond popped and indium started to melt.

3.3 HUMIDITY

The humidity tests were conducted at atmospheric pressure in a Hieatt chamber. Five bare detectors (two mounted on T05 cans, three mounted on flat packs made by Metallized Ceramic Corp) were stored in the chamber for 16 hours at $102^{\circ}\text{F} \pm 2^{\circ}\text{F}$ and relative humidity at $90\% \pm 4\%$ maintained by distilled water. After the exposure, two detectors with dark resistance $\sim 10^9 \Omega$, which were mounted on T05 can, were able to operate without degradation. The open terminal resistance of the flat pack on which the other three detectors were mounted was degraded to $10^9 \Omega$. After remount of the three detectors on a new flat pack, one detector was capable of operating without degradation. The other two detectors did not survive the remount process. The detector performance before and after the humidity test is summarized in Table 4.

3.4 SOLAR EXPOSURE

Five bare detectors mounted on flat packs were tested in direct sunlight. These measurements were made from 11:30 am to 2:30 pm on June 20, 1975 in Lexington, MA. The weather was clear with very light haze. The calculated incident solar energy from the sun angle at 12:30 pm for a perfectly clear day was 130 mW/cm^2 (based on $\text{AMO} = 139 \text{ mW/cm}^2$)⁽⁷⁾. Each detector was exposed to the solar radiation for periods of 1, 5, 10, and 15 minutes with recovery time noted after each increment time of exposure (see Figure 25). One can see that changing the duration of the solar exposure has little effect on the decay process. The decay process after solar exposure was characterized by an initial fast time constant and followed by a long decay time of several seconds.

There was no measureable change in detector performance before and after the solar exposure (see Table 5).

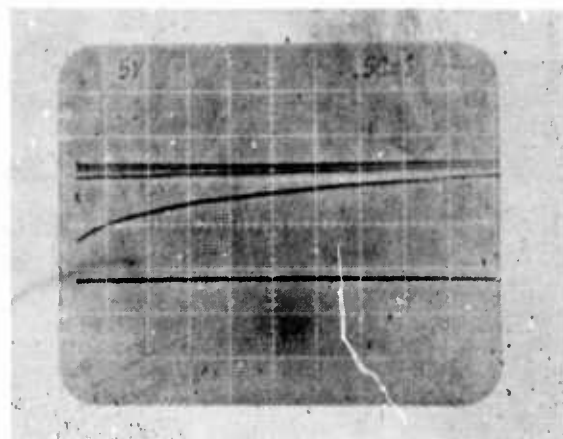
3.5 ELECTRON IRRADIATION

Three GaP:Cu slit detectors were evaluated before and after electron radiation. 1 MeV electron beam from a Van de Graaff accelerator at AFCRL was used. The beam intensity was set at $0.265 \mu\text{A/cm}^2\text{-s}$ ($1.66 \times 10^{12} \text{ e/cm}^2\text{-s}$). After a 606-s exposure, a total fluence of 10^{15} e/cm^2 was accumulated. For a 1 MeV electron beam, a dose rate of $1 \text{ e/cm}^2\text{-s}$ corresponds to $3.72 \times 10^{-8} \text{ rads/s}$. Therefore, a total dose of $3.72 \times 10^7 \text{ rads (Si)}$ was accumulated during the electron radiation test.

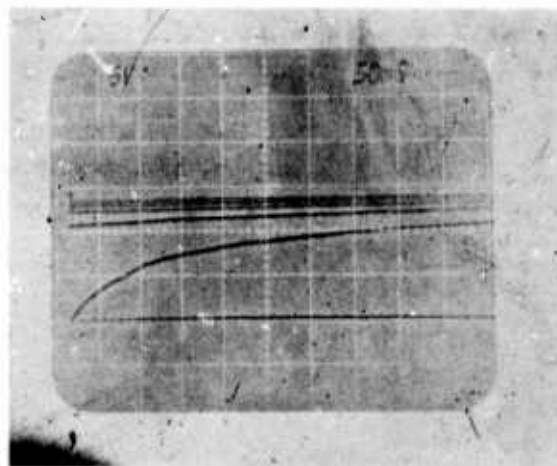
Table 4
HUMIDITY TEST

Detector	Dark Resistance Ω		Spot Scan Response		Noise V_N , pk-pk		Rise Time		Fall Time	
	Before	After	Before	After	Before	After	Before	After	Before	After
AD18-L16 No. 1	4.6×10^8	4.9×10^8	120 mV, at 0 m(V)	110 mV	20 mV	15 mV	70 ms	70 ms	80 ms	100 ms
AD18-L16 No. 2	4.7×10^8	3.8×10^8	60 mV at +0.75 m(V)	60 mV	20 mV	14 mV	80 ms	80 ms	80 ms	80 ms
AD25-M6A No. 1	1×10^{10}	5×10^9	700 mV at +1.2 m(V)	-	16 mV	-	1.1 s	-	3 s	-
AD15-M6A No. 2	3.9×10^{10}	1.5×10^{10}	400 mV at 0 m(V)	-	12 mV	-	400 ms	-	1 s	-
AD25-M6A No. 1	4.0×10^{10}	4.2×10^{10}	200 mV at +5 m(V)	180 mV	5 mV	5 mV	250 ms	250 ms	250 ms	250 ms

- Flat Packs Failed

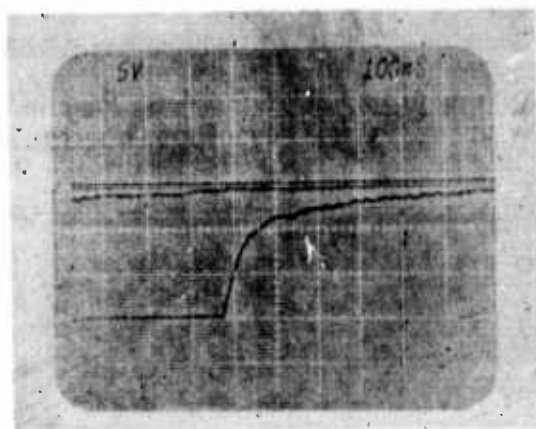


Detector AD18M8 No. 3|
Decay time after
1 min solar exposure



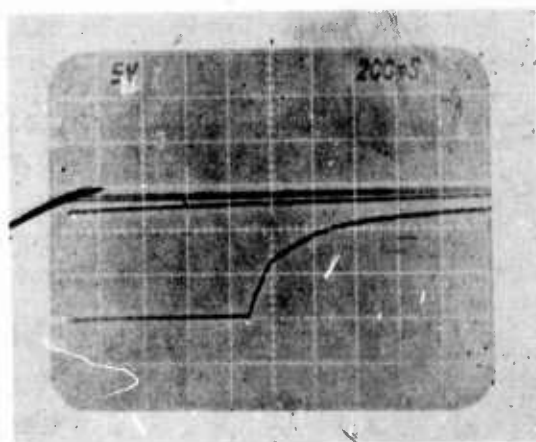
Decay time after
5 min solar exposure

Figure 25 DETECTOR DECAY TIME AFTER SOLAR EXPOSURE



Detector AD18M8 No. 3

Decay time after
10 min solar exposure



Decay time after
15 min solar exposure

Figure 25 (continued)

Table 5
DETECTOR PERFORMANCE BEFORE AND AFTER SOLAR EXPOSURE

Detector	Dark Resistance Ω		Spot Scan Response		Noise V_N , pk-pk		Rise Time		Fall Time	
	Before	After	Before	After	Before	After	Before	After	Before	After
AD25-M7 No. 1	2×10^{11}	2.4×10^{11}	30 mV +7.5 m(V)	30 mV	5 mV	5 mV	600 ms	700 ms	260 ms	240 ms
AD25-M7 No. 2	4.4×10^8	7.8×10^8	30 mV +2.5 m(V)	30 mV	6 mV	5 mV	400 ms	400 ms	240 ms	240 ms

The dark resistance, spot scan sensitivity and rise time of the three detectors before and after electron radiation are tabulated in Table 6. The most noticeable change is the detector rise time. Right after the electron exposure, the detector rise times are slower than before the electron radiation. Detector AD-25 M3 No. 1 was tested after being at room temperature for 70 hours. It exhibited less change than the two detectors which were tested immediately after the radiation. The dark resistance of those detectors measured within 70 hours after the electron radiation were about twice higher than that before. When measured four months after electron radiation, the dark resistance recovered to its initial value. We concluded that room temperature annealing caused this. In that case, long term dose accumulation in an in-space application would result in even greater radiation tolerance.

3.6 PROTON IRRADIATION

Three detectors were used for proton irradiation test. The test was performed by using AFCRL's linear accelerator. The beam intensity was set on the order of 10^{10} P/cm²-s and continuously monitored until a total dose of 10^{11} P/cm² was accumulated. The beam uniformity and the alignment of the sample holder were checked before the run. The detectors were capable of operating after the irradiation without any degradation (see Table 7).

3.7 GAMMA RAY EXPOSURE

Three detectors fabricated on this program were evaluated under gamma ray radiation.

To measure the gamma response of the GaP detectors, the detector and its preamplifier were placed inside a hot cell at AFCRL (Figure 26). A Victorian radiation-probe was positioned at approximately the same level and at approximately the same distance away from the source as the detector. This measured the gamma flux coming from the cobalt-60 source in terms of Roentgens per minute. The hot cell was sealed during the test and the detectors, mounted in T0-5 cans with open sleeve covers, were covered with black tape.

Preliminary checks were performed to assure that no noise was produced in the electronics or cabling while in a gamma environment.

Experiments were performed to characterize the response at room temperature of GaP photoconductors to 1 MeV gamma rays.

Table 6
DETECTOR PERFORMANCE BEFORE AND AFTER ELECTRON FLUENCE OF 10^{15} e/cm^2

Detector	Dark Resistance Ω		4 Month after irradiation	Spot Scan Sensitivity		Noise (pk-pk)		Rise Time	
	Before	Within 70 hrs. after irradiation		Before	Within 70 hrs. after irradiation	Before	Within 70 hrs. after irradiation	Before	After
AD18-L4 No. 1	2×10^8	5.6×10^8	2×10^8	50 mV	30 mV	600 μV	600 μV	200 ms	3 s
AD18-L12 No. 1	1.8×10^9	4.1×10^9	1.5×10^9	36 mV	22 mV	500 μV	800 μV	200 ms	600 ms
AD25-M3 No. 1	4×10^9	5×10^9	3.4×10^9	2.5 V	1.8 V	3.2 mV	4 mV	100 ms	200 ms

Table 7

DETECTOR PERFORMANCE BEFORE AND AFTER PROTON FLUENCE OF 10^{11} P/cm²

Detector	Dark Resistance Ω		Spot Scan Sensitivity		Noise (pk-pk)		Rise Time		Fall Time	
	Before	After	Before	After	Before	After	Before	After	Before	After
AD18-M7 No. 5	1.2×10^{11}	2.5×10^{11}	50 mV +5 m(V)	50 mV	4 mV	5 mV	50 ms	50 ms	70 ms	70 ms
AD18-M7 No. 6	2.3×10^{11}	4×10^{11}	80 mV +1.2 m(V)	90 mV	6 mV	7 mV	90 ms	90 ms	150 ms	120 ms
AD18-M7 No. 7	5.4×10^{11}	7×10^{11}	460 mS +5 m(V)	440 mV	1.6 mV	4 mV	2.2 s	2.2 s	150 ms	150 ms

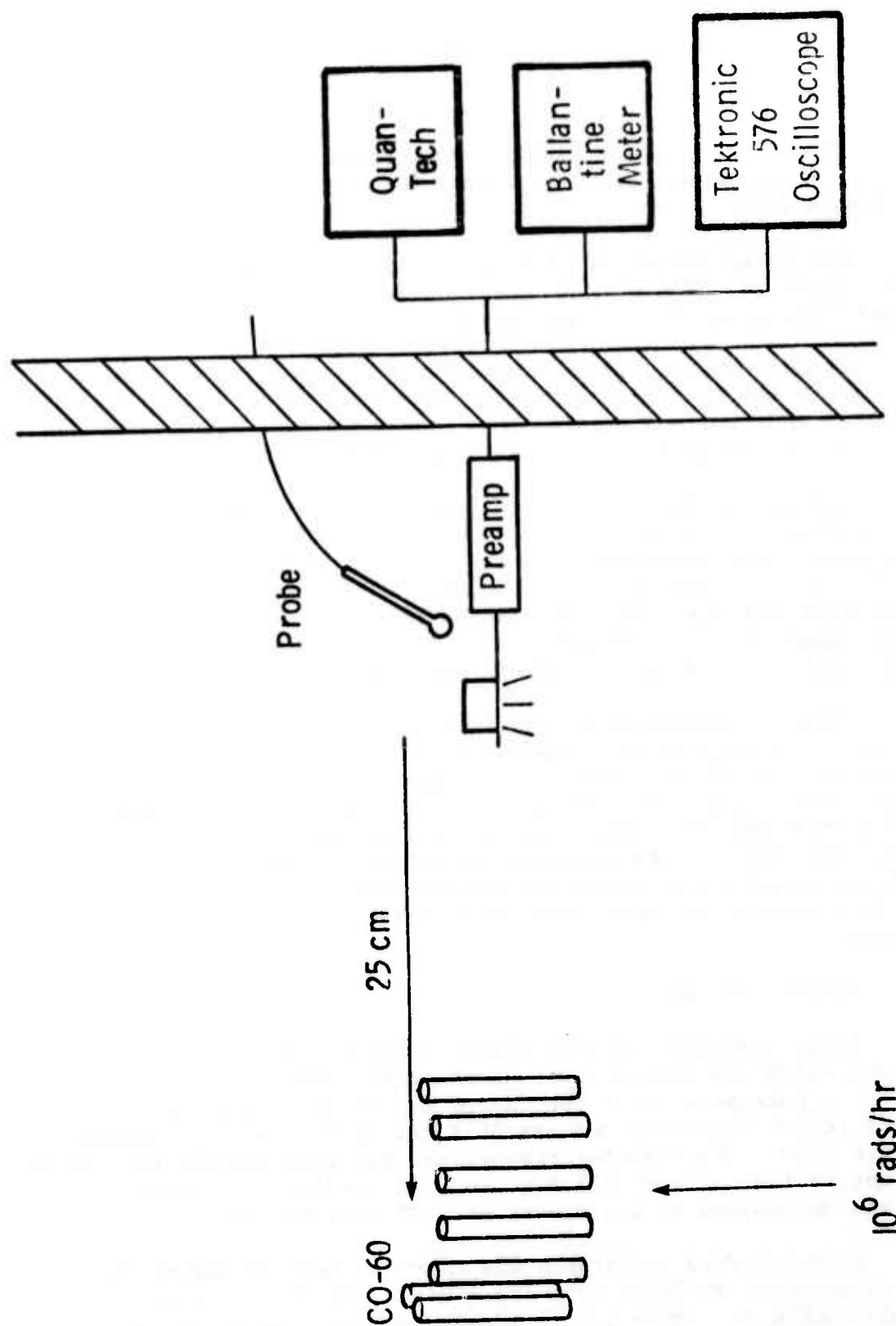


Figure 26 DETECTOR/PREAMP TESTING AT AFCRL CO-60 SOURCE

10^6 rads/hr

Figure 27 shows a typical gamma event response of a GaP detector. It is readily seen that the rise time is very fast. The delay time is about 8 ms.

Rms noise was measured as a function of gamma flux and is shown in Figure 28. There is no measureable increase in detector noise until the gamma flux is increased above $1 \times 10^6 \text{ } \gamma/\text{cm}^2\text{-s}$.

Figure 29 is a graph of event rate in pulses per second, as detected by the GaP photoconductive detector, versus gamma flux. The slope of this curve indicates that the event rate of the detector is directly proportional to the gamma flux, as expected.

During the gamma radiation test, detector dark resistance was measured with a Keithley meter 602 as a function of gamma flux. The dark resistance was decreased by a factor of 10 when the gamma flux reached $1.5 \times 10^{10} \text{ } \gamma/\text{cm}^2\text{-s}$. With the same experimental setup, an Eltec resistor was measured. It changed by a factor of two under the same high gamma flux (see Figure 30). This suggests that there may be a radiation-induced current in the measuring circuit.

Three photoconductive GaP detectors (AD18L17 No. 1, AD18L17 No. 2, AD18L-9B) were exposed to a cobalt source with a total dose of 1×10^6 rads over a 6 - 7 hour period. The dark resistance, spot scan sensitivity, rms noise, and rise time were measured before and after the gamma radiation dose for each individual detector. The results are tabulated in Table 8. One can see that there is not measureable change before and after radiation exposure and GaP is indeed a radiation-hard semiconductor material at these dose levels.

3.8 THERMAL VACUUM

Eight Cu-doped GaP slit detectors were used in the thermal vacuum test which was run in a vacuum chamber. The detectors were mounted on a Honeywell built test apparatus which automatically cycles the tested detectors between 30°F and 160°F every 90 minutes (see Figure 31). The detector temperature was continuously monitored for the entire test period (151.5 hours, 101 cycles). The test chamber was maintained at a pressure of 10^{-6} torr or less.

Detector dark resistance was taken before and during the thermal vacuum test at 30°F, 70°F and 160°F. The results were tabulated in Table 9. There was no evidence of any electrical or mechanical deterioration. We believe that the slight reduction (about 10%) of detector resistance at 160°F is not due to the thermal effect, i.e., increase of bulk carrier concentration as temperature

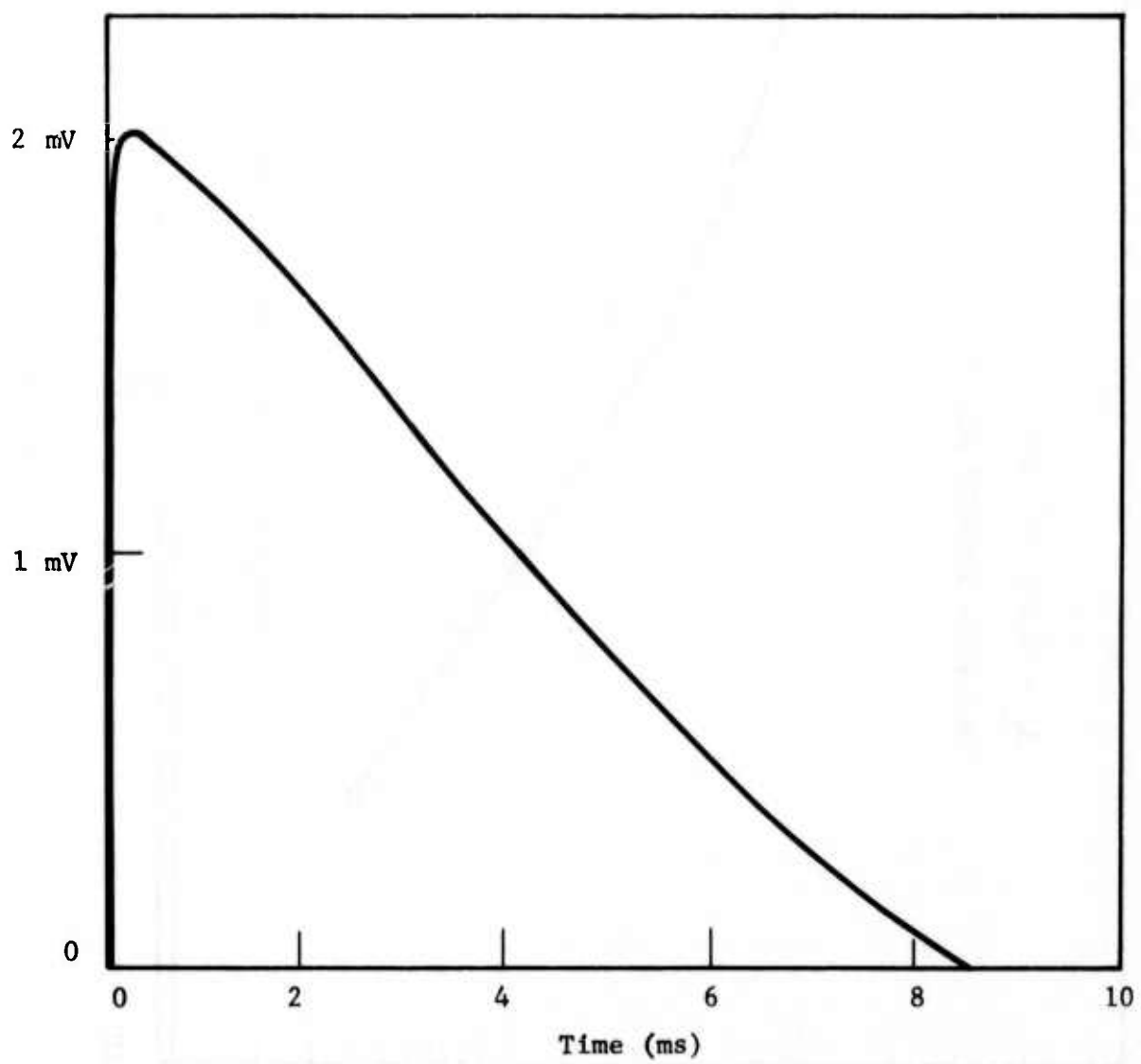


Figure 27 DETECTOR RESPONSE TO A GAMMA EVENT

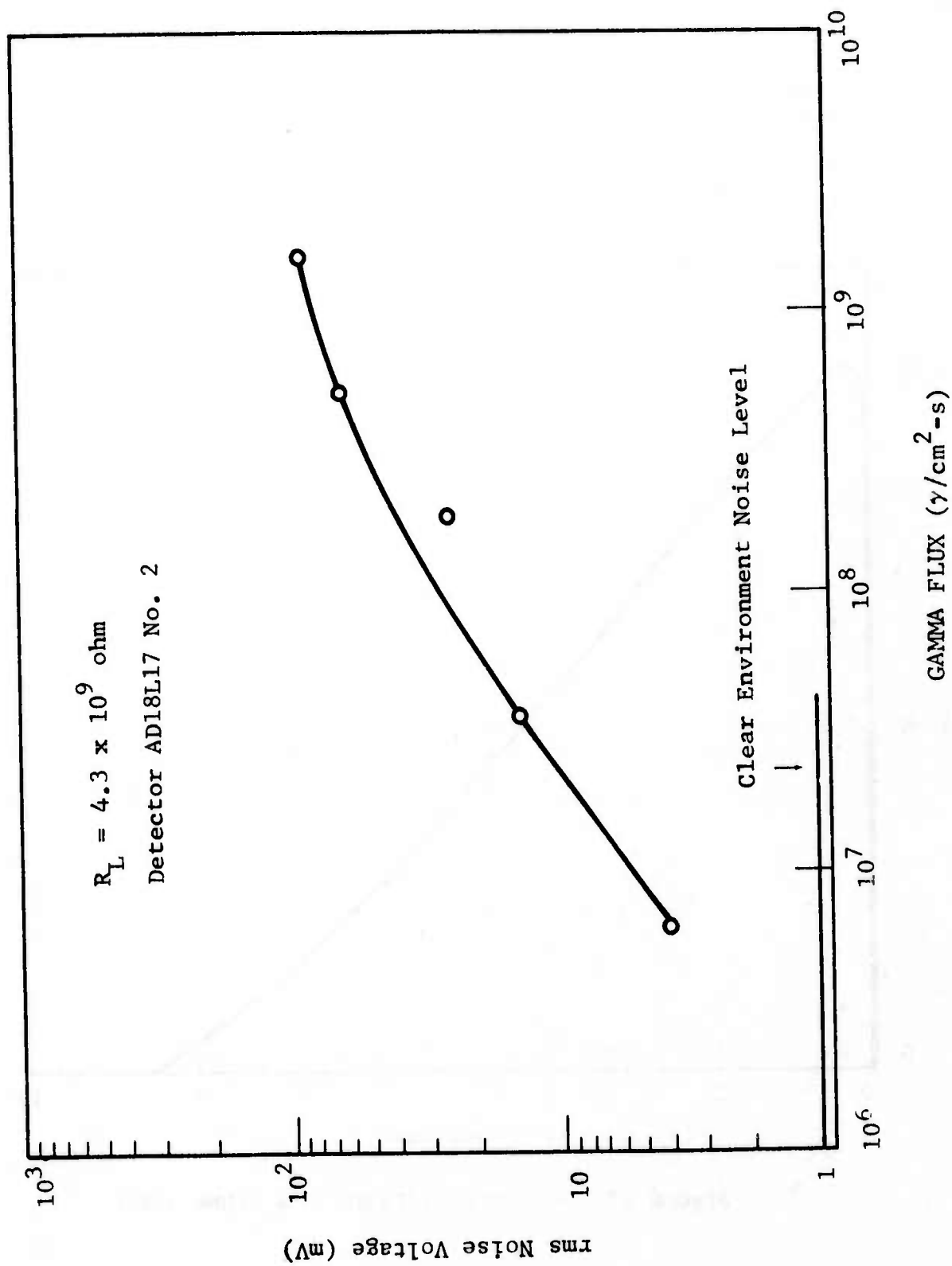


Figure 28 DETECTOR NOISE VS GAMMA FLUX

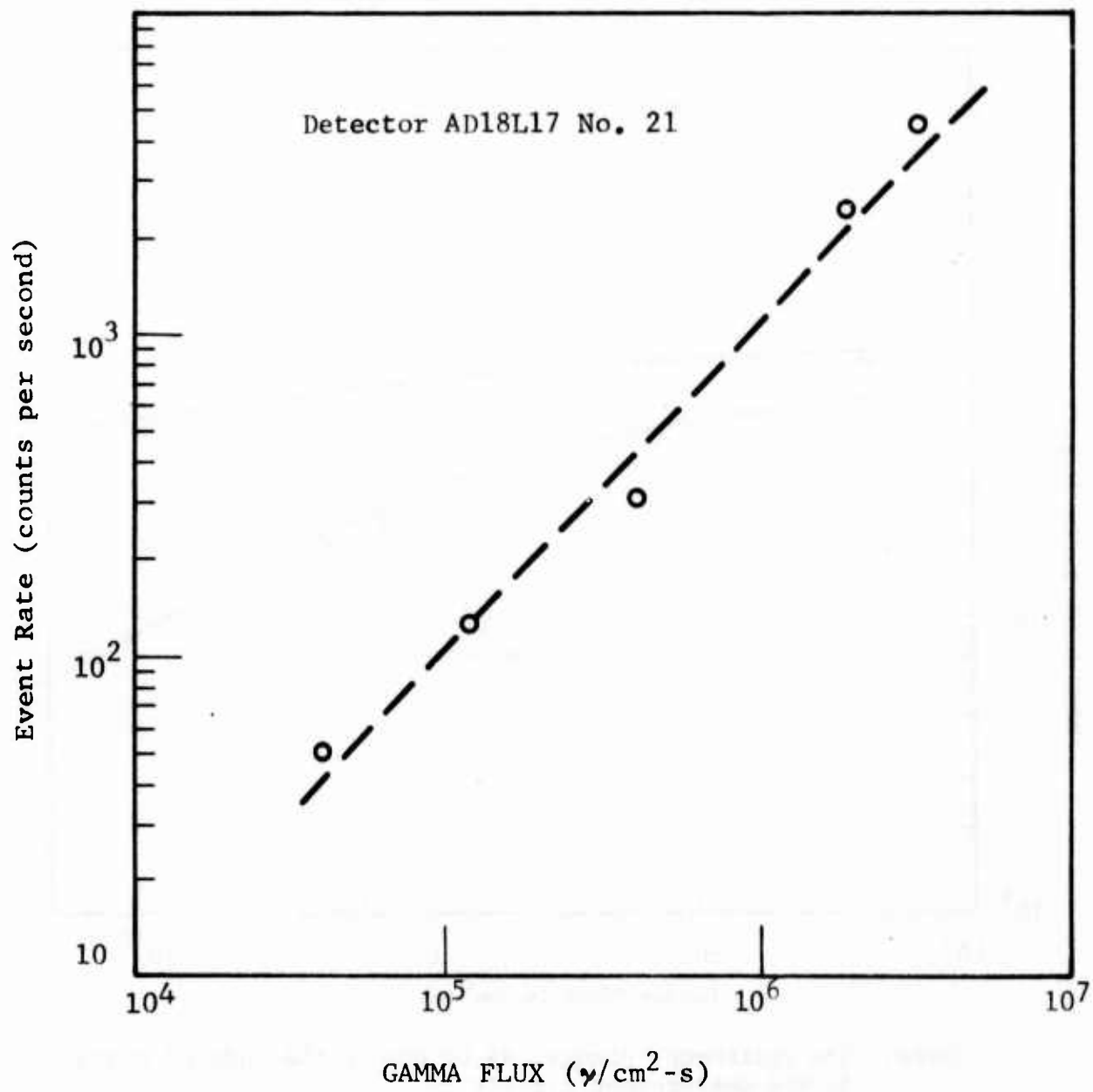
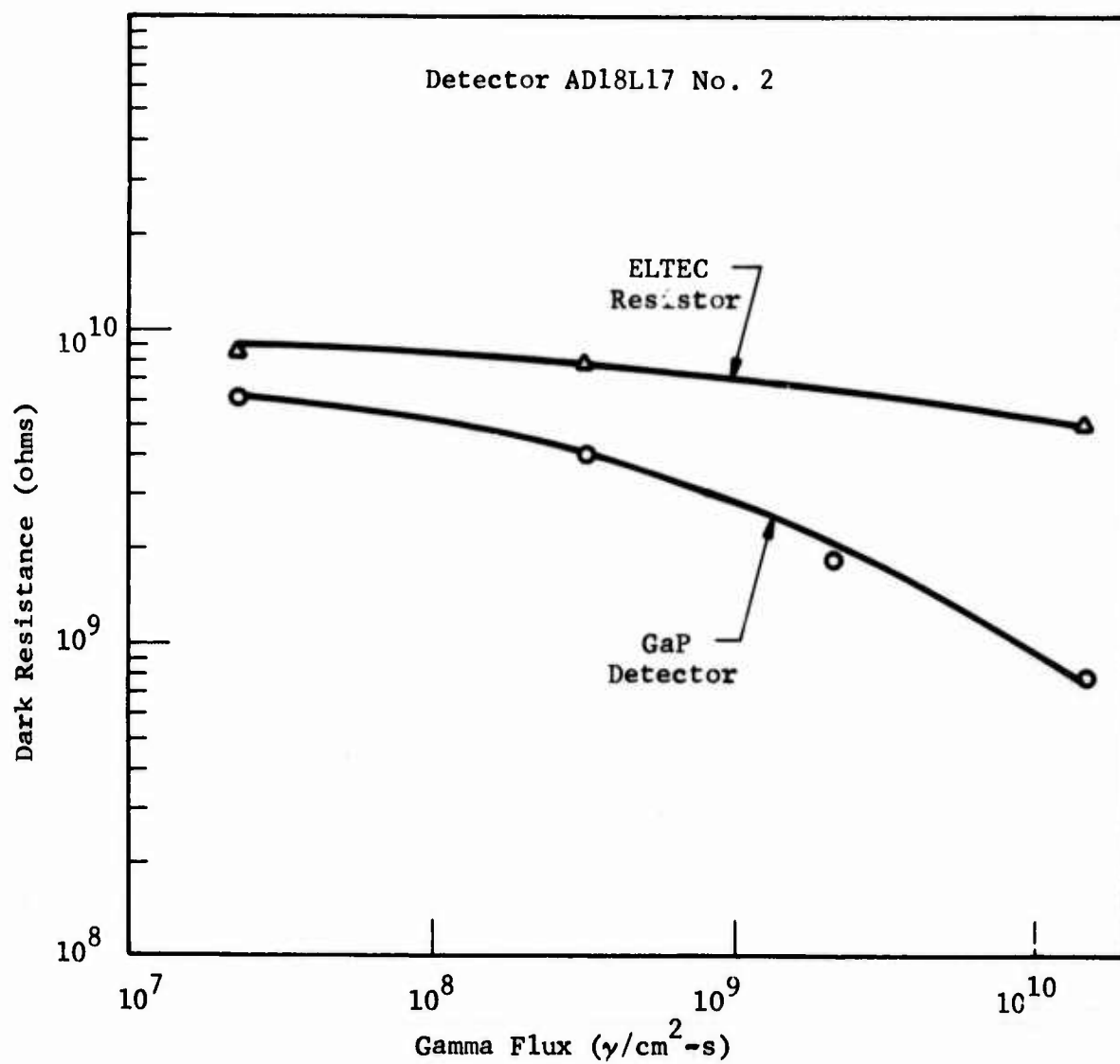


Figure 29 DETECTOR EVENT RATE VS GAMMA FLUX



Note: The resistance change may be due to the induced current in the measurement circuit

Figure 30 DETECTOR DARK RESISTANCE VS GAMMA FLUX

Table 8
GAMMA RADIATION EXPOSURE
(total dose = 1×10^6 rads)

Detector ID	Dark Resistance		Spot Scan Signal +2 m(V)		Noise (rms)		Rise Time	
	Before	After	Before	After	Before	After	Before	After
AD18-A17 No. 1	4.2×10^{10}	4.0×10^{10}	25 mV	25 mV	420 μ V	440 μ V	200 ms	200 ms
AD18-L17 No. 2	1.0×10^{10}	9.0×10^9	120 mV	150 mV	1.0 mV	1.1 mV	80 ms	80 ms
AD18-L19 No. 3	1.4×10^8	1.4×10^8	40 mV	40 mV	3.8 mV	3.8 mV	60 ms	60 ms

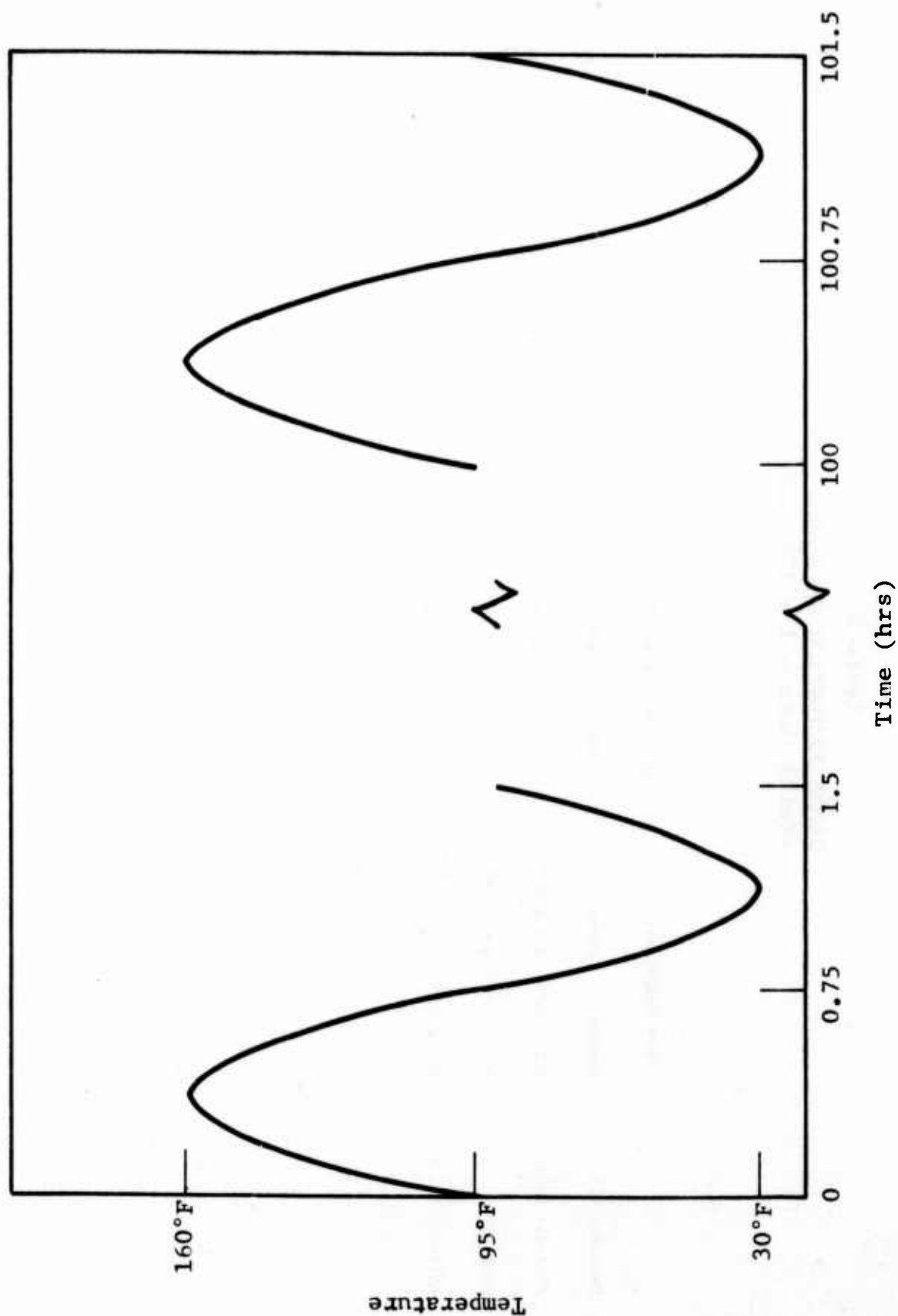


Figure 31 THERMAL VACUUM TEST TEMPERATURE PROFILE

Table 9
DARK RESISTANCE MEASUREMENT DURING THERMAL VACUUM TEST

	Dark Resistance (ohm) Before Thermal Vacuum	Dark Resistance (ohm) During Thermal Vacuum (7-30-75) at 30°F at 70°F		Dark Resistance (ohm) During Thermal Vacuum (8-4-75) at 30°F at 70°F	
		at 160°F (Heater on)		at 160°F (Heater on)	
AD18-W7 No. 1	7×10^{11}	6×10^{11}	6×10^{11}	6×10^{11}	8×10^{10}
AD18-W7 No. 2	2.45×10^{11}	2.9×10^{11}	3×10^{11}	2.2×10^{11}	4×10^{10}
AD18-W7 No. 3	9×10^{10}	9×10^{10}	8.5×10^{10}	9×10^{10}	8.9×10^{10}
AD18-W7 No. 4	1.8×10^{11}	2.5×10^{11}	3.2×10^{11}	2×10^{11}	4×10^{10}
AD18-W7 No. 8	5.4×10^9	3.9×10^9	3.6×10^9	1.7×10^9	7×10^8
AD18-W7 No. 9	3.2×10^{11}	4.1×10^{11}	4.9×10^{11}	6.5×10^{11}	3.7×10^{11}
AD24-L1 No. 1	8×10^5	8×10^5	7.1×10^5	8×10^5	7.4×10^5
AD24-L1 No. 4	9.4×10^8	9×10^6	8.6×10^6	9×10^6	8.5×10^6

Table 9 (Cont.)

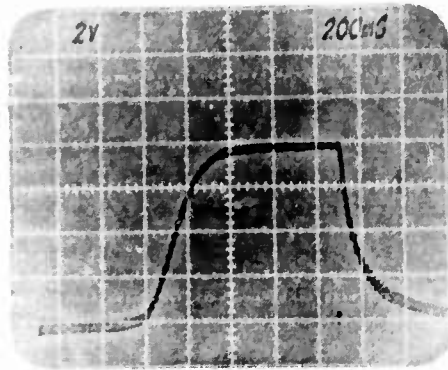
DARK RESISTANCE MEASUREMENT AT THERMAL VACUUM TEST

	Dark Resistance During Thermal Vacuum (8-5-75)			Dark Resistance After Thermal Vacuum
	at 30°F	at 70°F	at 160°F	
AD18-M7 No. 1	6×10^{11}	1.6×10^{11}	1×10^{11}	6×10^{11}
AD18-M7 No. 2	3×10^{11}	2×10^{11}	4.5×10^{10}	2.4×10^{11}
AD18-M7 No. 3	9.4×10^{10}	9×10^{10}	8×10^{10}	9×10^{10}
AD18-M7 No. 4	3.5×10^{11}	2.4×10^{11}	3.5×10^{10}	3.2×10^{11}
AD18-M7 No. 8	1.4×10^9	1×10^9	7×10^8	2.8×10^9
AD18-M7 No. 9	6.5×10^{11}	5.1×10^{11}	3.4×10^{11}	5.7×10^{11}
AD24-L1 No. 1	8.2×10^5	8.1×10^5	7.9×10^5	7×10^5
AD24-L1 No. 4	9×10^6	8.5×10^6	8.5×10^6	8.6×10^6

is increased. The heating apparatus includes an electric heater. While the thermal cycle was at 160°F, the heater was on and glowed red. The glowing heater acted as an optical light source and generated free electrons in the detector and reduced the detector resistance.

An initial electrical test was performed. Because the amplifier was not kept inside the chamber during the thermal vacuum cycling, the detector output was connected to the input terminal of the amplifier through long (about 10 ft) shielded cables. Excess noise was produced in the cables. Therefore, for this test only relative signal data before, during and after the thermal vacuum were reported.

A small light bulb was placed inside the shield dark chamber. Signals through the amplifier were taken before, after, and during the thermal vacuum cycle at 30°F, 70°F and 160°F (see Figure 32). One can easily see that there is no performance variation at different temperature points.



Detector AD18M7 No. 9
Signal before thermal
vacuum cycle

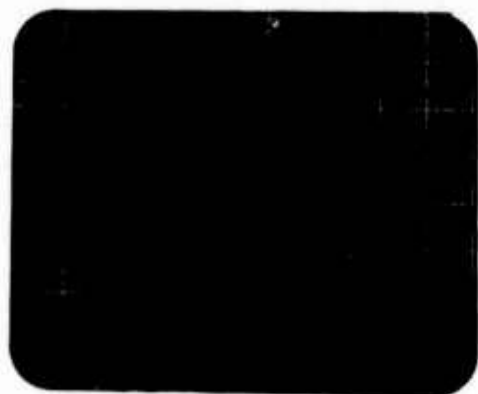


Signal during thermal
vacuum cycle at 30°F

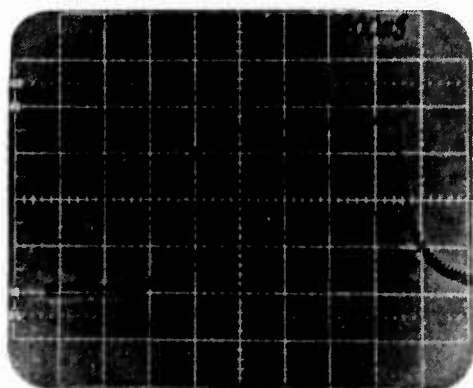


Signal during thermal
vacuum cycle at 75°F

Figure 32 DETECTOR SIGNAL DURING THERMAL VACUUM TEST



Detector AD18M7 No. 9
Signal during thermal
vacuum cycle at 160°F



Signal after thermal vacuum
cycle at room temperature

Figure 32 (continued)

SECTION IV

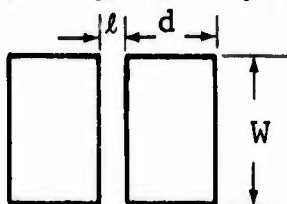
SUMMARY

Cu-doped GaP photoconductive slit detectors with the dimensions $0.05 \times 0.0005 \text{ inch}^2$ have been developed for star sensor applications. The sensitivity of these devices approaches the performance of photomultipliers, and their response times are faster than those of CdS and CdSe. For example, noise equivalent powers as low as $6 \times 10^{-16} \text{ W}/\sqrt{\text{Hz}}$ at $0.5 \text{ } \mu\text{m}$ and corner frequencies as high as 50 Hz have been observed on these devices. The GaP photoconductive detectors are environmentally stable and exhibit high radiation resistance. Test results obtained on this program indicated that Cu-doped GaP slit detectors exhibit no permanent degradation after exposure to 200°F ; $90\% \pm 4\%$ relative humidity; vibration from 400 to 3,000 Hz under 25 g; electron irradiation to 10^{15} e/cm^2 ; proton irradiation to 10^{11} p/cm^2 ; and gamma ray exposure to 10^6 rads (Si) . The lack of spot scan uniformity along the slits is the chief drawback of these devices. Therefore, for the photoconductive mode Cu-doped GaP detectors, further material growth development effort is required to achieve accurate compensation, reproducibility and uniformity.

APPENDIX

CALCULATION OF DARK RESISTANCE OF A SLIT DETECTOR WITH PARALLEL PLATE ELECTRODE CONFIGURATION

A parallel plate electrode configuration sketched below is used to make contact to the slit detectors, where ℓ , W are the slit width any length, respectively, and d is the width of the electrodes.



The dark resistance, when there is no incident light flux, is equivalent to the volume shunt which can be calculated from electrostatic theory.⁽¹⁾

$$R_d = \frac{K\left(\frac{\ell}{2d+\ell}\right)}{\sigma_d W K\left(\frac{2d^{1/2}(d+\ell)^{1/2}}{2d+\ell}\right)} \quad (1)$$

where σ_d is the bulk conductivity of the material and $K(k)$ is a complete elliptic integral of modulus k . For the present program, the slit detector has dimensions ℓ , d , $W = 0.5$, 3.5 , 50 mils, respectively, the calculated dark resistance from equation 1 is

$$R_d = \frac{2.8}{\sigma_d} \quad (2)$$

REFERENCES

1. R.A. Rotolante, et al, "Advanced Slit Detectors for Star Sensors." Technical Report AFAL-TR-74-353 (1974).
2. B. Goldstein and S. Periman "Electrical & Optical Properties of High Resistivity Gallium Phosphide" Phys. Rev. 148, 715 (1966).
3. H. Grimmeiss and G. Olofsson "Charge-Carrier Capture and its Effect on Transition Capacitance in GaP-Cu Diodes" J. of Appl. Phys. 40, 2526 (1969).
4. D. Bowman "Photoconductive and Photo Hall Measurements on High Resistivity GaP" J. Appl. Phys. 38, 568 (1967).
5. R. Schulze and P. Peterson "Photoconductivity in Solution Grown Cu-doped GaP" J. of Appl. Phys. 45, 5307 (1974).
6. P.J. Dean, G. Kamincký and R. Zetterstorm, J. Appl. Phys. 38, 3551 (1967).
7. Y. Nannichi and G. Pearson "Properties of GaP Schottky Barrier Diode at Elevated Temperature" Solid State Electronics, 12, 341 (1969).
8. M.P. Thekaekara "Data on Incident Solar Energy Technical Information Service, American Institute of Aeronautics and Astronautics.

UNCLASSIFIED

AD BD 17183

AUTHORITY:

AFWAL

10, 19 OCT 81



UNCLASSIFIED